ELSEVIER

Comput. Methods Appl. Mech. Engrg. 180 (1999) 1–26

Computer methods in applied mechanics and engineering

www.elsevier.com/locate/cma

Finite element analysis of nonsmooth contact

C. Kane, E.A. Repetto, M. Ortiz *, J.E. Marsden

California Institute of Technology, Mail Stop 105-50, Pasadena, CA 91125, USA

Received 29 January 1998; received in revised form 8 September 1998

Abstract

This work develops robust contact algorithms capable of dealing with complex contact situations involving several bodies with corners. Amongst the mathematical tools we bring to bear on the problem is nonsmooth analysis, following Clarke (F.H. Clarke. Optimization and nonsmooth analysis. John Wiley and Sons, New York, 1983.). We specifically address contact geometries for which both the use of normals and gap functions have difficulties and therefore precludes the application of most contact algorithms proposed to date. Such situations arise in applications such as fragmentation, where angular fragments undergo complex collision sequences before they scatter. We demonstrate the robustness and versatility of the nonsmooth contact algorithms developed in this paper with the aid of selected two and three-dimensional applications.

1. Introduction

The objective of the work presented in this paper is the development of robust contact algorithms capable of dealing with multibody nonsmooth contact geometries for which neither normals nor gap functions can be defined. Such situations arise in many areas of application and are exemplified by granular flows and by brittle solids undergoing fragmentation. Dynamic fragmentation often results in the formation of large numbers of fragments which undergo complex collision sequences before they eventually scatter [10,36]. During the initial stages of fragmentation, the corners of many angular fragments come together at a point, Fig. 1, which precludes the definition of a proper gap function as a means of detecting – and constraining – the interpenetration of the fragments. In addition, because of the nonsmooth character of the fragments, normals cannot be uniquely defined in the contact region. Because fragments are tightly packed initially, contact situations such as shown in Fig. 1 arise which involve potential collisions between a large number of bodies. A robust and systematic procedure is therefore required in order to ascertain the precise sequence of collisions undergone by the bodies. We refer to contact processes such as described, involving the simultaneous interaction between many angular bodies, as *nonsmooth contact*.

Most contact algorithms proposed to date envision two smooth bodies in contact and use a gap function to constrain or penalize interpenetration (see, e.g., Refs. [4,12,5,2,18,33,34,42,17,43,30,44,45,55,26–28,31,40,22,11,53,39,52,49,32,48,59,60,65,66,62,56,61,57,64,58,63]). These approaches are not applicable to the analysis of nonsmooth contact. We show in the sequel that, once equipped with the right mathematical tools, it is indeed possible – and straightforward – to formulate powerful nonsmooth contact algorithms. The appropriate mathematical framework is furnished by *nonsmooth analysis* (see Ref. [14]), which provides a general characterization of the contact forces arising in nonsmooth contact problems; and the analytical

* Corresponding author. Fax: +1 626 395-4530.
E-mail address: ortiz@madrid.caltech.edu (M. Ortiz)

0045-7825/99/$ - see front matter
PII: S0045-7825(99)00034-1

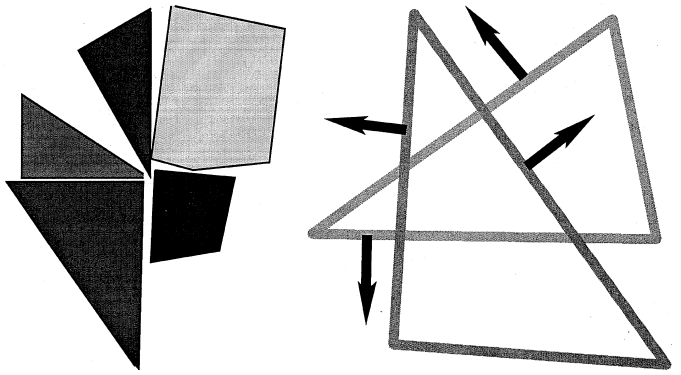

Fig. 1. Examples of nonsmooth contact. (a) Confluence of several angular solids at a point; (b) two overlapping angular fragments.

tools required for formulating and effectively treating time-discretized approximations. Similar tools have recently been applied by Schuricht [67,68] to the analysis of elastic rods in obstacle problems.

The resulting algorithms bear a noteworthy resemblance to those which are suggested by the mathematical theory of plasticity (see, e.g., Ref. [35,37,41]), specially as regards the use of *closest-point projections*, an analogy which has been noted by Laursen and Govindjee [69]. However, it should be noted that the admissible sets which arise in contact problems are generally *nonconvex*, which precludes the direct application of convex analysis.

The organization of the paper is as follows. In Section 2 we briefly review the salient aspects of nonsmooth analysis which are relevant to contact. Because in this paper we are specifically interested in the finite element analysis of nonsmooth contact, we confine our review to the finite dimensional case. A parallel development of nonsmooth contact in a functional setting may be found elsewhere [23]. In Section 3, a theory of nonsmooth contact algorithms is developed. The theory applies to two and three dimensions and to static and dynamic problems. Finally, in Section 4 the robustness and versatility of the algorithms is demonstrated with the aid of selected examples.

2. Finite-dimensional nonsmooth analysis

Je me détourne avec effroi et horreur de cette plaie lamentable des fonctions qui n'ont pas de dérivées. Hermite in a letter to Stieltjes (cf. Ref. [14], comments on Chapter 2).

We begin by reviewing a few basic concepts of nonsmooth analysis used in subsequent derivations. A complete account on nonsmooth analysis may be found in the monograph [14]. In essence, nonsmooth analysis deals with physical objects and functions for which strict differentiability may not be postulated. In particular, one of the goals of nonsmooth analysis is to develop a collection of tools enabling the study of differential properties of nondifferentiable functions.

Let $X = \mathbb{R}^n$ equipped with the euclidean norm $\|\cdot\|$. We identify the dual space X^* with $\mathbb{R}^n$ itself, and denote the duality pairing $\langle \cdot, \cdot \rangle$. Physically, X is to be regarded as the space of positions and velocities, whereas X^* is the space of forces. The duality pairing $\langle \boldsymbol{f}, \boldsymbol{v} \rangle$, $\boldsymbol{v} \in X, \boldsymbol{f} \in X^*$, is then the power developed as a point moves with velocity $\boldsymbol{v}$ under the action of force $\boldsymbol{f}$. Throughout this section, unless otherwise stated a function $f(\boldsymbol{x})$ will be understood to be defined over X and to take values over the real line $\mathbb{R}$.

Let Y be a subset of X. A function f is said to be *Lipschitz* of rank K over Y if

$$|f(\boldsymbol{y}) - f(\boldsymbol{x})| \leqslant K\|\boldsymbol{y} - \boldsymbol{x}\| \tag{2.1}$$

for all points $\boldsymbol{x}$, $\boldsymbol{y}$ in Y. A Lipschitz function near a point $\boldsymbol{x}$ need not be differentiable at that point. However, in finite dimensions, Rademacher's Theorem states that a function which is Lipschitz in an open subset of R^n is differentiable almost everywhere (in the sense of Lebesgue measure) on that subset.

Let f be Lipschitz near a point $\boldsymbol{x}$ and let $\boldsymbol{v}$ be a vector in X. The *generalized directional derivative* of f at $\boldsymbol{x}$ in the direction $\boldsymbol{v}$ is

$$f^{\circ}(\boldsymbol{x};\boldsymbol{v}) = \limsup_{\boldsymbol{y}\to\boldsymbol{x},t\to 0^{+}} \frac{f(\boldsymbol{y}+t\boldsymbol{v}) - f(\boldsymbol{y})}{t}, \tag{2.2}$$

where $\boldsymbol{y} \in X$ and t is a positive scalar. This definition generalizes the conventional concept of directional derivative in that it does not presuppose the existence of any limits, as it involves the upper limit only, and the base point $\boldsymbol{y}$ is allowed to vary.

The *generalized differential (aka gradient)* of a Lipschitz function f at $\boldsymbol{x}$ is the subset of X^{*} given by

$$\partial f(\boldsymbol{x}) = \{\boldsymbol{f} \in X^{*} \mid f^{\circ}(\boldsymbol{x};\boldsymbol{v}) \geqslant \langle \boldsymbol{f}, \boldsymbol{v}\rangle, \text{ for all } \boldsymbol{v} \in X\}. \tag{2.3}$$

The generalized directional derivative is recovered from the generalized gradient as

$$f^{\circ}(\boldsymbol{x};\boldsymbol{v}) = \max\{\langle \boldsymbol{f}, \boldsymbol{v}\rangle \mid \boldsymbol{f} \in \partial f(\boldsymbol{x})\}. \tag{2.4}$$

The generalized gradient reduces to the ordinary derivative at points where the function is continuously differentiable. It also reduces to the subdifferential in the case of convex functions.

A simple example of application of the above concepts is the *absolute value function* $f(x) = |x|$ in $X = \mathbb{R}$. This function is not differentiable at the origin in the ordinary sense. However, a straightforward calculation gives $f^{\circ}(0;v) = |v|$ and $\partial f(0) = [-1,1]$. Thus, both the generalized directional derivative and the generalized gradient are defined at the origin.

Generalized directional derivatives and gradients provide a means of characterizing local minima of nonsmooth functions. Let f be a Lipschitz function. The notion of a local minimum of f is defined in the usual way. The following proposition provides a condition that minima must satisfy in terms of generalized gradients; the proof proceeds in a way parallel to the proof in smooth calculus and may be found in Ref. [14, p. 38].

Proposition 2.1. *Let f be Lipschitz. If $\boldsymbol{x}$ is a local minimum of f, then*

$$\boldsymbol{0} \in \partial f(\boldsymbol{x}). \tag{2.5}$$

There are a number of connections between nonsmooth analysis and geometry which will prove useful in contact applications. We begin by considering a nonempty subset $C \subset X$ and defining the *distance function* as

$$d_C(\boldsymbol{x}) = \inf\{\|\boldsymbol{x} - \boldsymbol{y}\| \mid \boldsymbol{y} \in C\}. \tag{2.6}$$

This function is globally Lipschitz of rank 1 but not differentiable in the classical sense. The distance function $d_C(\boldsymbol{x})$ provides a useful device for characterizing certain aspects of the geometry of C. For instance, the *tangent cone* $T_C(\boldsymbol{x})$ to C at $\boldsymbol{x}$ is the set

$$T_C(\boldsymbol{x}) = \{\boldsymbol{v} \in X \mid d_C^{\circ}(\boldsymbol{x};\boldsymbol{v}) = 0\}. \tag{2.7}$$

The *normal cone* $N_C(\boldsymbol{x})$ to C at $\boldsymbol{x}$ is defined by polarity as

$$N_C(\boldsymbol{x}) = \{\boldsymbol{f} \in X^{*} \mid \langle \boldsymbol{f}, \boldsymbol{v}\rangle \leqslant 0, \text{ for all } \boldsymbol{v} \in T_C(\boldsymbol{x})\}. \tag{2.8}$$

Fig. 2 gives an example of a tangent and a normal cone at a convex point. For us, we will also need to consider nonconvex points as well; examples of tangent and normal cones in this case are depicted in Fig. 3. We refer to Ref. [14] for the techniques for computing these (the definition as given is not always the most convenient way). Evidently, if $\boldsymbol{x}$ is in the interior of C then $T_C(\boldsymbol{x}) = X$ and $N_C(\boldsymbol{x}) = \{\boldsymbol{0}\}$. Furthermore, if C is closed and $\boldsymbol{x}$ is a regular (i.e., smooth) point of ∂C then $T_C(\boldsymbol{x})$ is the interior tangent halfspace to C at $\boldsymbol{x}$ and $N_C(\boldsymbol{x})$ is the outward normal ray.

Clarke [14] has shown how generalized gradients and the related concepts outlined above can be extended to functions which are not locally Lipschitz and take values in the extended real line $\mathbb{R} \cup \{\pm\infty\}$. A detailed discussion of this extension is beyond the scope of this brief account. However, a particular class of

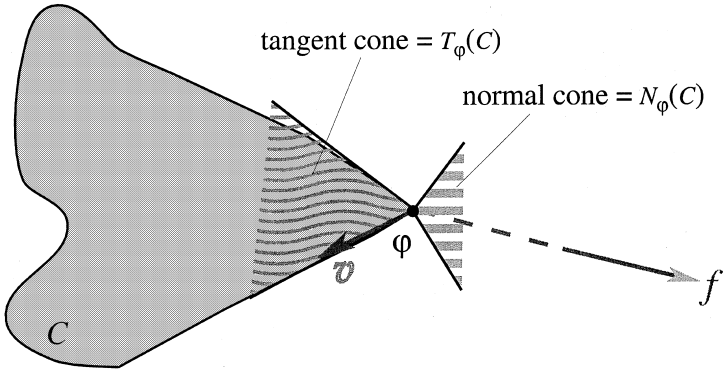

Fig. 2. The tangent and normal cones.

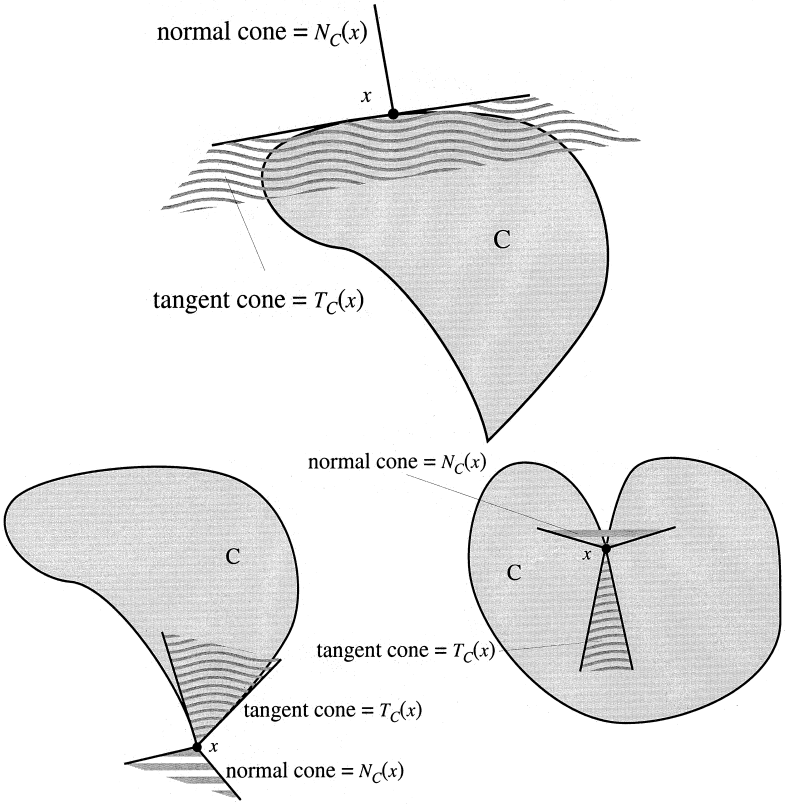

Fig. 3. Examples of tangent and normal cones for some smooth and nonsmooth geometries.

such extended functions, the so called *indicator functions*, merits discussions as it will play a central role in the characterization of contact forces in nonsmooth problems.

The *indicator* of a set C in X is the extended-valued function:

$$I_C(\boldsymbol{x}) = \begin{cases} 0 & \text{if } \boldsymbol{x} \in C, \\ \infty & \text{otherwise.} \end{cases} \tag{2.9}$$

Let $\boldsymbol{x} \in C$. Then it follows that

$$\partial I_C(\boldsymbol{x}) = N_C(\boldsymbol{x}), \quad \boldsymbol{x} \in C, \tag{2.10}$$

i.e., the generalized differential of the indicator function at $\boldsymbol{x} \in C$ coincides with the normal cone at $\boldsymbol{x}$.

The set identity (2.10) establishes an important connection between generalized gradients and geometry. Another such connection may be effected by introducing the concept of *closest point projection*. In formulating time-discretization algorithms for contact, the closest point projection provides the canonical means for returning deformed configurations to the admissible set.

Begin by defining the *resolvent* of ∂I_C as the set-valued mapping

$$R_{\partial I_C} = (I + \partial I_C)^{-1}. \tag{2.11}$$

Thus, one has that $\boldsymbol{x} \in R_{\partial I_C}(\boldsymbol{y})$ iff $\boldsymbol{y} \in \boldsymbol{x} + \partial I_C(\boldsymbol{x})$. Resolvents play an important role in the approximation theory of nonlinear semigroups of operators (e.g., Refs. [24,25,15,9,16,8]) and, in particular, in the mathematical theory of plasticity (see, e.g., Ref. [35]).

The resolvent of an operator is simply the mapping resulting from an application of the backward Euler algorithm to the equation of evolution defined by the operator. A central result for dissipative systems, which are characterized by operators which are maximal monotone [8], is that the resolvent mapping is contractive and, consequently, the backward Euler algorithm is unconditionally stable. For a convex set C the operator ∂I_C is indeed maximal monotone [8]. For instance, a consequence of this fact is that the closest point return mapping stress update algorithm for ideal plasticity is unconditionally stable [35,37,41].

Now let C be a set in X and $\boldsymbol{y}$ be a point in X. The *closest-point projection* of $\boldsymbol{y}$ onto C is the set

$$P_C(\boldsymbol{y}) = \{\boldsymbol{x} \in \mathrm{cl}C \mid \ d_C(\boldsymbol{y}) = \|\boldsymbol{x} - \boldsymbol{y}\|\} \tag{2.12}$$

It follows from the definition that $P_C^2 = P_C$ and, therefore, P_C does indeed define a nonlinear projection from X onto the closure of C. Evidently, if C is closed then $P_C(\boldsymbol{y})$ reduces to the singleton $\{\boldsymbol{y}\}$ iff $\boldsymbol{y} \in C$. For a convex set C, the corresponding closest-point projection P_C is uniquely defined and maps X onto C. However, P_C is generally set-valued for arbitrary nonconvex sets.

It is a well-known fact that the resolvent of the subgradient of the indicator function of a convex set is the closet-point projection onto that set [47,35] (see Fig. 4). For general sets, a similar connection is established by the following proposition.

Proposition 2.2. *Let C be a nonempty subset of X. Then*

$$R_{\partial I_C} \supset P_C. \tag{2.13}$$

Proof. Let $\boldsymbol{y} \in X$. Then $\boldsymbol{x} \in P_C(\boldsymbol{y})$ iff it is a minimum of the extended function $f(\boldsymbol{x}) = \|\boldsymbol{x} - \boldsymbol{y}\| + I_C(\boldsymbol{x})$, where the second term in effect restricts $\boldsymbol{x}$ to C. By Proposition 2.1, if $\boldsymbol{x}$ is a local minimum of f, then $\boldsymbol{0} \in \partial f(\boldsymbol{x}) = (\boldsymbol{x} - \boldsymbol{y})/\|\boldsymbol{x} - \boldsymbol{y}\| + \partial I_C(\boldsymbol{x})$. Since by (2.10) $\partial I_C(\boldsymbol{x})$ is a cone, this holds iff $\boldsymbol{y} - \boldsymbol{x} \in \partial I_C(\boldsymbol{x})$. □

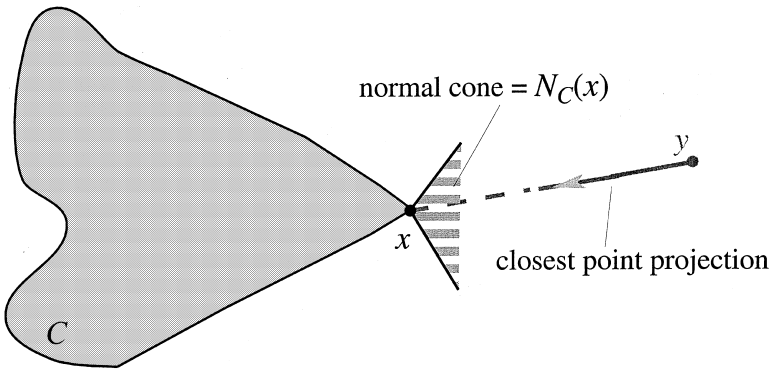

Fig. 4. The projection of a point onto a set near a convex point.

3. Nonsmooth contact algorithms

Next, we turn to the application of the above analytical tools to the problem of nonsmooth contact. Our main focus is the development of nonsmooth contact algorithms in a finite element context and, consequently, we confine our attention to the finite-dimensional case. A parallel development of a theory of nonsmooth contact in a functional setting may be found elsewhere [23].

We shall be concerned with the motions of a deformable solid occupying a domain $B_0 \subset R^d$ in its reference configuration. The deformations of interest are described by deformation mappings $\boldsymbol{\varphi}_h : B_{0h} \times [0,T] \to R^d$ subordinate to a finite element discretization of B_0. Here $[0,T]$ is the time duration of the motion. For a fixed $t \in [0,T]$, the deformation mappings $\boldsymbol{\varphi}_h(\cdot,t)$ define a finite-dimensional space X_h. By a slight abuse of notation, we shall variously take $\boldsymbol{\varphi}_h$ to denote the discretized deformation field or the array of nodal coordinates in the deformed configuration. For simplicity, we shall assume the solid to be elastic. Extensions to inelasticity may be effected simply by the introduction of incremental energy densities such as described in Ref. [46].

3.1. The unconstrained case

In the absence of contact constraints, the action functional for the solid is of the form

$$I[\boldsymbol{\varphi}_h] = \int_0^T \left[\frac{1}{2} \dot{\phi}_h^T \boldsymbol{M}_{\mathrm{h}} \dot{\boldsymbol{\varphi}}_h - \phi(\boldsymbol{\varphi}_h) + \boldsymbol{f}^{\mathrm{ext}} \cdot \boldsymbol{\varphi}_h \right] \mathrm{d}t \tag{3.1}$$

where $\boldsymbol{M}_{\mathrm{h}}$ is the mass matrix of the solid, $\phi(\boldsymbol{\varphi}_h)$ denotes its strain energy and $\boldsymbol{f}^{\mathrm{ext}}(t)$ are the externally applied forces. The equations of motion of the spatially discretized solid follow by requiring that $I[\boldsymbol{\varphi}_h]$ be stationary, with the result

$$\boldsymbol{M}_{\mathrm{h}} \ddot{\boldsymbol{\varphi}}_h + \boldsymbol{f}^{\mathrm{int}}(\boldsymbol{\varphi}_h) = \boldsymbol{f}^{\mathrm{ext}} \tag{3.2}$$

where

$$\boldsymbol{f}^{\mathrm{int}} = \nabla \phi(\boldsymbol{\varphi}_h) \tag{3.3}$$

are the internal forces. Eq. (3.2), in conjunction with initial conditions of the form

$$[\boldsymbol{\varphi}_h]_{t=0} = \boldsymbol{\varphi}_{h0}, \tag{3.4}$$

$$\left[\dot{\boldsymbol{\varphi}}_h\right]_{t=0} = \dot{\boldsymbol{\varphi}}_{h0}, \tag{3.5}$$

defines an initial value problem to be solved for $\boldsymbol{\varphi}_h$.

3.2. Time discretization – unconstrained case

We shall envision an incremental solution procedure whereby $\boldsymbol{\varphi}_h$ is approximated at discrete times $t_n = n\Delta t$. For definiteness, we specifically consider time-discretization algorithms belonging to Newmark's family [6,21]. Other time-discretization algorithms may be treated similarly. The time-discretized equations of motion are, therefore, of the form

$$\boldsymbol{\varphi}_{n+1} = \boldsymbol{\varphi}_n + \Delta t\, \dot{\boldsymbol{\varphi}}_n + \Delta t^2 \left[(1/2 - \beta) \ddot{\boldsymbol{\varphi}}_n + \beta \ddot{\boldsymbol{\varphi}}_{n+1} \right], \tag{3.6}$$

$$\dot{\boldsymbol{\varphi}}_{n+1} = \dot{\boldsymbol{\varphi}}_n + \Delta t \left[(1-\gamma) \ddot{\boldsymbol{\varphi}}_n + \gamma \ddot{\boldsymbol{\varphi}}_{n+1} \right], \tag{3.7}$$

$$\boldsymbol{M}_h \ddot{\boldsymbol{\varphi}}_{n+1} + \boldsymbol{f}^{\mathrm{int}}(\boldsymbol{\varphi}_{n+1}) = \boldsymbol{f}^{\mathrm{ext}}_{n+1}, \tag{3.8}$$

which defines a system of nonlinear equations to be solved for $\boldsymbol{\varphi}_{n+1}$, $\dot{\boldsymbol{\varphi}}_{n+1}$ and $\ddot{\boldsymbol{\varphi}}_{n+1}$.

To complete the specification of our contact algorithm, we shall first develop some geometric and analytic tools.

3.3. The admissible set

Our aim now is to extend the above solution procedure to nonsmooth contact problems. The notion of an *admissible set* of deformations will play a central role to that effect. The admissible set $C_h \subset X_h$ is simply the set of all globally invertible deformation mappings in X_h. Physically, $\boldsymbol{\varphi}_h \in C_h$ iff the deformation mapping $\boldsymbol{\varphi}_h$ does not entail interpenetration of matter, Fig. 5.

Consider, as an elementary example, the case of two point masses undergoing rectilinear motion, Fig. 6. Let the position of the masses be x_1 and x_2 and assume that the trailing particle cannot overtake the leading particle. The configuration space of this system is then $X = R^2$ and consists of all pairs (x_1, x_2), while the admissible set C is simply the half-plane $x_2 \geqslant x_1$, Fig. 6.

A second elementary but particularly enlightening example is furnished by a particle in a rigid box, Fig. 7. In this case, the configuration space is also $X = R^2$ and the admissible set C is the box itself. This example illustrates an important point, namely, that *the admissible set need not be convex*. Indeed, for the geometry depicted in Fig. 7, it is clear that while configurations $\boldsymbol{x}_A$ and $\boldsymbol{x}_B$ are both admissible, certain convex combinations $(1-\lambda)\boldsymbol{x}_A + \lambda \boldsymbol{x}_B$ fall outside the containing box and are therefore not admissible. The example of a particle in a box also serves to illustrate the lack of smoothness resulting from the presence of corners. Other analytically tractable examples may be found in Ref. [23].

Next we turn to the definition of the admissible set C_h for spatially discretized deformation mappings.

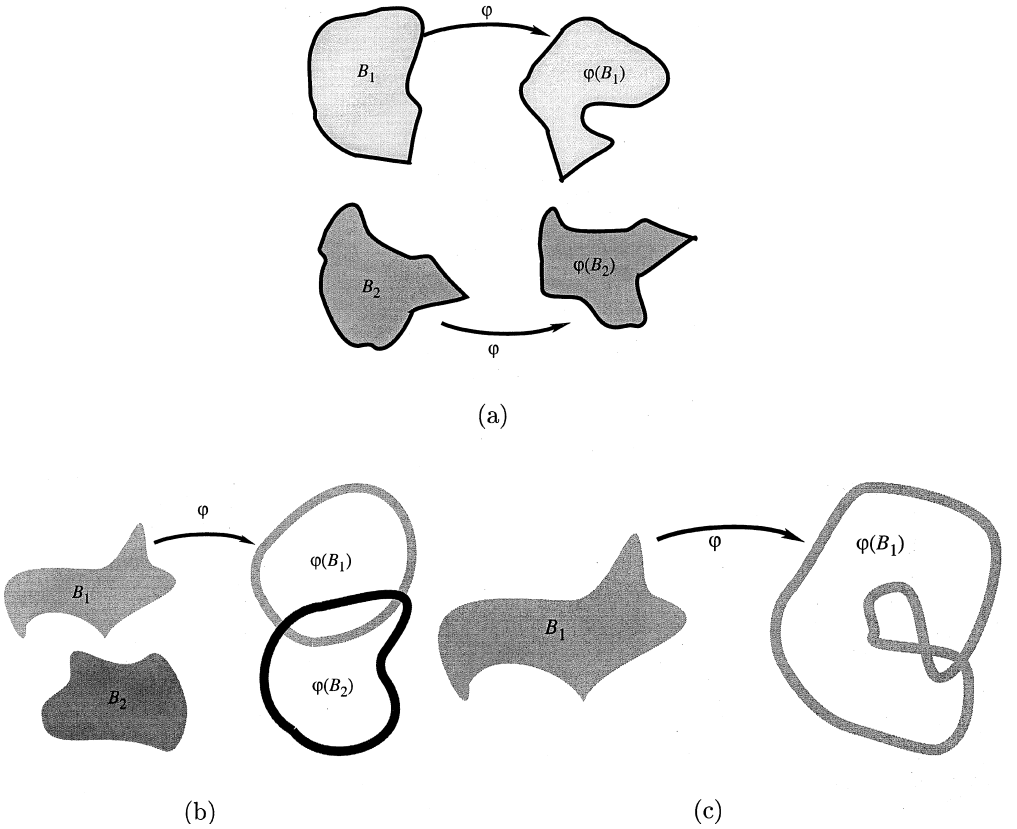

Fig. 5. Definition of the set C of admissible deformations. (a) Example of an admissible deformation not entailing interpenetration of matter. (b) Example of a deformation which is not admissible due to penetration between two bodies. (c) Example of a deformation which fails to be admissible due to interpenetration of two parts of the same body.

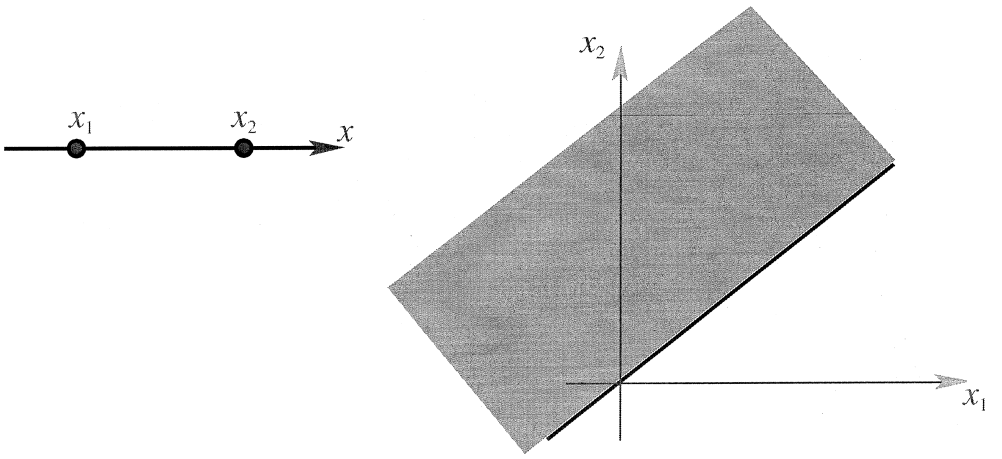

Fig. 6. The admissible set for the elementary example of two particles undergoing rectilinear motion, with the trailing particle unable to overtake the leading particle.

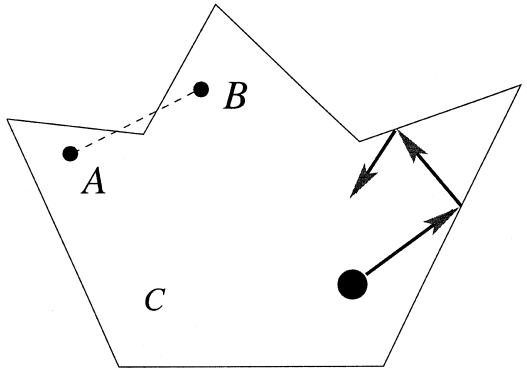

Fig. 7. The motion of a particle in a rigid box, illustrating the lack of convexity and smoothness of contact problems in the presence of corners.

The two dimensional case. We start by considering the case of two-dimensional bodies. The boundary of a two-dimensional body of finite perimeter may be decomposed into a collection of closed loops [20]. Each of these loops constitutes a one-dimensional manifold without boundary and the collection of all loops can be oriented consistently so as to unambiguously define the interior and the exterior of each body [20]. We conventionally take the outer loop of each body to be oriented counterclockwise, and the inner loops clockwise, so that the interior of the body is to the left of the loops. Upon spatial discretization, the loops comprising the boundary ∂B_h of the deformed configuration B_h are themselves discretized into oriented closed segments Γ. These segments define a triangulation $\mathscr{S}_h$ of ∂B_h.

Evidently, a necessary and sufficient condition for the interpenetration of matter to occur is that the interior of two deformed boundary segments intersect, Fig. 8. This leads to the following definition of the admissible set of deformations:

$$C_h = \{\boldsymbol{\varphi}_h \in X_h \mid \mathrm{Int}(\Gamma_1) \cap \mathrm{Int}(\Gamma_2) = \varnothing, \text{ for all } \Gamma_1, \Gamma_2 \in \mathscr{S}_h, \Gamma_1 \neq \Gamma_2\}, \tag{3.9}$$

where $\mathrm{Int}(\Gamma)$ is the one-dimensional interior of segment Γ, i. e., the open segment with the end-points excluded. Note that so far we have succeeded at avoiding the use of normals and gap functions.

An analytical definition of C_h which preserves this situation is the following. For simplicity, we consider the case of linear segments. Let the index α label pairs of distinct segments in $\mathscr{S}_h$. Thus, if $\mathrm{card}(\mathscr{S}_h)$ is the number of boundary segments, then $N = \mathrm{card}(\mathscr{S}_h)[\mathrm{card}(\mathscr{S}_h) - 1]/2$ is the number of such pairs. For each

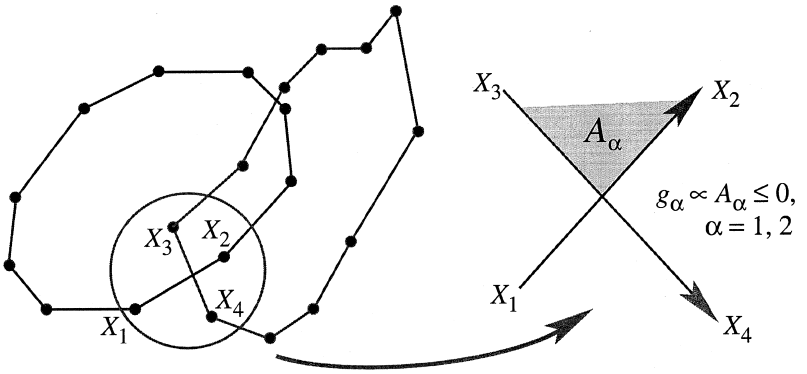

Fig. 8. Analytical formulation of nonsmooth contact constraints.

intersecting pair α we define a constraint function g_α as follows. We recall that all boundary pairs are oriented. This enables the determination of an area A_α which is negative when interpenetration takes place, as shown in Fig. 8.

Conversely, the constraint that $A_\alpha \geqslant 0$ excludes the possibility of interpenetration of the pair of segments α. A convenient choice of constraint function is $g_\alpha \propto A_\alpha$. As stated, g_α is a rational function of the coordinates of the end points of the segments. However, as discussed in Appendix A, the constraint condition can be manipulated algebraically and recast in a polynomial form, Eq. (A.2).

In terms of these constraint functions, the admissible set can now be defined as:

$$C_h = \{\boldsymbol{\varphi}_h \in X_h \mid g_\alpha(\boldsymbol{\varphi}_h) \geqslant 0,\ \alpha = 1, \ldots, N\} \tag{3.10}$$

Again we emphasize that neither normals nor gap functions are used in the definition of C_h. In particular, the definition applies to such nonsmooth contact situations as depicted in Fig. 1, as required.

The three dimensional case. The three-dimensional case may be treated similarly. The boundary of a three-dimensional body of finite surface area may be decomposed into a collection of shells [20]. Each of these shells constitutes a two-dimensional manifold without boundary and the collection of all shells can be oriented consistently so as to unambiguously define the interior and the exterior of each body [20], as in Fig. 9. Upon spatial discretization, the shells comprising ∂B_h are themselves discretized into oriented closed faces Γ. These faces define a triangulation $\mathscr{S}_h$ of ∂B_h.

Interpenetration occurs iff the interior of two deformed boundary faces intersect, as in Fig. 9. This leads to the same definition (3.9) of the admissible set of deformations as in the two-dimensional case, again

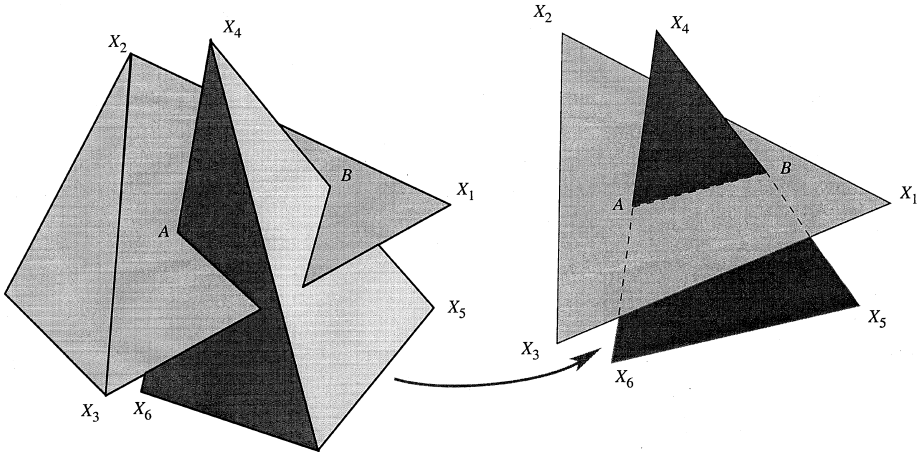

Fig. 9. Constraints associated with the intersection of tetrahedra in space.

without recourse to normals or gap functions. In this context, $\mathrm{Int}(\Gamma)$ is to be interpreted as the two-dimensional interior of face Γ, i.e., the open face with its boundary segments excluded.

In the simple case of planar faces, an analytical definition of C_h may be obtained as follows. Let the index α now label pairs of distinct faces in $\mathscr{S}_h$. For each intersecting pair α we define a constraint function g_α as follows. Using the face orientation, we identify a volume V_α which is negative when interpenetration takes place, and reduces to zero when interpenetration is removed, as in Fig. 9. A convenient choice of constraint function is, therefore, $g_\alpha \propto V_\alpha$. As in the two-dimensional case, g_α can be simplified and put into polynomial form, see Section A.2.

In terms of these constraint functions, the admissible set can now be defined in the form (3.10). Again we stress that neither normals nor gap functions are used in the definition of C_h.

We close this section by noting that C_h is invariant under the action of translations and rotations. Thus, if the deformation mapping $\boldsymbol{\varphi}_h \in C_h$, i.e., if $\boldsymbol{\varphi}_h$ is globally invertible, then it is evident that the deformation mappings $\boldsymbol{\varphi}_h + \boldsymbol{c}$ and $\boldsymbol{R}\boldsymbol{\varphi}_h$ are also globally invertible for all translations $\boldsymbol{c} \in R^d$ and all rotations $\boldsymbol{R} \in SO(d)$, and, consequently, they are in C_h. These invariance properties of C_h are born out by the analytical parametrization (3.10). Indeed, the constraint functions g_α represent interpenetration areas (volumes) between pairs of segments (faces) in two (three) dimensions and are therefore invariant with respect to superposed translations and rotations.

3.4. The constrained case

Next we turn to the numerical treatment of nonsmooth contact problems. As is commonly done in so-called *barrier* methods, the interpenetration constraint may be accounted for by adding the term $I_{C_h}(\boldsymbol{\varphi}_h)$ to the energy of the solid, whereupon the action functional becomes

$$I(\boldsymbol{\varphi}_h) = \int_0^{\mathrm{T}} \left[\frac{1}{2} \dot{\boldsymbol{\varphi}}_{\mathrm{h}}^{\mathrm{T}} \boldsymbol{M}_{\mathrm{h}} \dot{\boldsymbol{\varphi}}_{\mathrm{h}} - \phi(\boldsymbol{\varphi}_{\mathrm{h}}) - \mathrm{I}_{\mathrm{C_h}}(\boldsymbol{\varphi}_{\mathrm{h}}) + \boldsymbol{f}^{\mathrm{ext}} \cdot \boldsymbol{\varphi}_{\mathrm{h}} \right] \mathrm{dt}. \tag{3.11}$$

Evidently, from definition (2.9) of the indicator function of a set it follows that the additional term in the energy effectively bars the trajectories from exiting the admissible set C_h, i.e., from violating the interpenetration constraint.

The problem is now to determine the absolutely continuous trajectories $\boldsymbol{\varphi}_h(t)$ which render the action stationary (cf. Ref. [14]). From the stationarity condition (2.5) it follows that the trajectories are weak solutions of the equation

$$\boldsymbol{0} \in \boldsymbol{M}_{\mathrm{h}} \ddot{\boldsymbol{\varphi}}_h + \boldsymbol{f}^{\mathrm{int}}(\boldsymbol{\varphi}_h) + \partial I_{C_h}(\boldsymbol{\varphi}_h) - \boldsymbol{f}^{\mathrm{ext}}. \tag{3.12}$$

Eq. (3.12), in conjunction with initial conditions (3.5) and (3.6), defines an initial value problem to be solved for $\boldsymbol{\varphi}_h$. In Eq. (3.12), the term $\partial I_{C_h}(\boldsymbol{\varphi}_h)$ amounts to the contact forces over configuration $\boldsymbol{\varphi}_h$.

It follows from the invariance properties of C_h that I_{C_h}, and by extension the action I, is itself invariant under the action of translations and rotations. It therefore follows from Noether's theorem (see, e.g., Ref. [29]) that the solutions of (3.12) conserve linear and angular momentum. Global energy conservation follows likewise from the time independence or autonomous character of the lagrangian. Additionally, since any admissible solution must necessarily be such that $I_{C_h}(\boldsymbol{\varphi}_h(t)) = 0$, which corresponds to the fact that the contact area does not store or dissipate energy, it follows that the volume energy is also conserved.

3.5. A class of nonsmooth contact algorithms

A class of time-stepping algorithms may now be obtained by treating (3.12) within the framework of the Newmark family of algorithms defined in Eqs. (3.6)–(3.8). As in the case of plasticity (see, e.g., Refs. [38,37,41]), the robustness of the algorithm requires a fully *implicit* treatment of the contact force system $\partial I_{C_h}(\boldsymbol{\varphi}_h)$. By contrast, the remainder of the terms in (3.12) may be treated either *implicitly* or *explicitly*. In view of this distinction, we split the accelerations into terms due to the internal and contact forces, with the result

$$\ddot{\boldsymbol{\varphi}}_h = \ddot{\boldsymbol{\varphi}}_h^{\text{int}} + \ddot{\boldsymbol{\varphi}}_h^{\text{con}}, \tag{3.13}$$

where

$$\ddot{\boldsymbol{\varphi}}_h^{\text{int}} = \boldsymbol{M}_{\text{h}}^{-1}[\boldsymbol{f}^{\text{ext}} - \boldsymbol{f}^{\text{int}}(\boldsymbol{\varphi}_h)], \tag{3.14}$$

$$\ddot{\boldsymbol{\varphi}}_h^{\text{con}} = -\boldsymbol{M}_{\text{h}}^{-1}\partial I_{C_h}(\boldsymbol{\varphi}_h). \tag{3.15}$$

A general class of *implicit/explicit* algorithms is obtained by setting:

$$\boldsymbol{\varphi}_{n+1} = \boldsymbol{\varphi}_n + \Delta t\,\dot{\boldsymbol{\varphi}}_n + \Delta t^2[(1/2-\beta)\ddot{\boldsymbol{\varphi}}_n^{\text{int}} + \beta\ddot{\boldsymbol{\varphi}}_{n+1}^{\text{int}}] + (\Delta t^2/2)\ddot{\boldsymbol{\varphi}}_{n+1}^{\text{con}}, \tag{3.16}$$

$$\dot{\boldsymbol{\varphi}}_{n+1} = \dot{\boldsymbol{\varphi}}_n + \Delta t\,[(1-\gamma)\ddot{\boldsymbol{\varphi}}_n^{\text{int}} + \gamma\ddot{\boldsymbol{\varphi}}_{n+1}^{\text{int}}] + \Delta t\ddot{\boldsymbol{\varphi}}_{n+1}^{\text{con}}. \tag{3.17}$$

The *explicit/implicit* member of the algorithm, i.e., that which is explicit in the internal forces and implicit in the contact forces, corresponds to the choice $\beta = 0$. We shall refer to the remaining members as being *implicit/implicit*.

The above relations may be simplified by introducing the notation

$$\boldsymbol{\varphi}_{n+1}^{\text{pre}} = \boldsymbol{\varphi}_n + \Delta t\,\dot{\boldsymbol{\varphi}}_n + (1/2-\beta)\Delta t^2\ddot{\boldsymbol{\varphi}}_n^{\text{int}}, \tag{3.18}$$

whereupon (3.16) becomes

$$\boldsymbol{\varphi}_{n+1} = \boldsymbol{\varphi}_{n+1}^{\text{pre}} + \beta\Delta t^2\ddot{\boldsymbol{\varphi}}_{n+1}^{\text{int}} + (\Delta t^2/2)\ddot{\boldsymbol{\varphi}}_{n+1}^{\text{con}}. \tag{3.19}$$

Making use of the equation of motion (3.12), (3.19) may be recast in the form

$$\boldsymbol{0} \in \boldsymbol{M}_{\text{h}}(\boldsymbol{\varphi}_{n+1} - \boldsymbol{\varphi}_{n+1}^{\text{pre}}) + \beta\Delta t^2[\boldsymbol{f}^{\text{int}}(\boldsymbol{\varphi}_{n+1}) - \boldsymbol{f}_{n+1}^{\text{ext}}] + (\Delta t^2/2)\partial I_{C_h}(\boldsymbol{\varphi}_{n+1}) \tag{3.20}$$

which defines a system of nonlinear algebraic equations to be solved for $\boldsymbol{\varphi}_{n+1}$. Once this solution is effected, the internal accelerations $\ddot{\boldsymbol{\varphi}}_{n+1}^{\text{int}}$ follow from (3.14) and the contact accelerations from (3.20), with the result

$$\ddot{\boldsymbol{\varphi}}_{n+1}^{\text{con}} = \frac{2}{\Delta t^2}(\boldsymbol{\varphi}_{n+1} - \boldsymbol{\varphi}_{n+1}^{\text{pre}}) - 2\beta\ddot{\boldsymbol{\varphi}}_{n+1}^{\text{int}}. \tag{3.21}$$

Finally, the velocities are computed from (3.17), which completes an application of the algorithm.

3.6. Variational structure

The crux of the algorithm just described consists of the determination of $\boldsymbol{\varphi}_{n+1}$ from (3.20). The variational structure of this problem may be ascertained as follows. Begin by noting that (3.20) may be written in the form

$$\boldsymbol{0} \in \partial f(\boldsymbol{\varphi}_{n+1}) + \partial I_{C_h}(\boldsymbol{\varphi}_{n+1}), \tag{3.22}$$

where

$$f(\boldsymbol{\varphi}_{n+1}) = \frac{1}{\Delta t^2}(\boldsymbol{\varphi}_{n+1} - \boldsymbol{\varphi}_{n+1}^{\text{pre}})\boldsymbol{M}_{\text{h}}(\boldsymbol{\varphi}_{n+1} - \boldsymbol{\varphi}_{n+1}^{\text{pre}}) + 2\beta[\phi(\boldsymbol{\varphi}_{n+1}) - \boldsymbol{f}_{n+1}^{\text{ext}} \cdot \boldsymbol{\varphi}_{n+1}]. \tag{3.23}$$

In the explicit case, $\beta = 0$, and

$$f(\boldsymbol{\varphi}_{n+1}) = \frac{1}{\Delta t^2}(\boldsymbol{\varphi}_{n+1} - \boldsymbol{\varphi}_{n+1}^{\text{pre}})\boldsymbol{M}_{\text{h}}(\boldsymbol{\varphi}_{n+1} - \boldsymbol{\varphi}_{n+1}^{\text{pre}}) = \|\boldsymbol{\varphi}_{n+1} - \boldsymbol{\varphi}_{n+1}^{\text{pre}}\|_K^2, \tag{3.24}$$

where

$$\|\boldsymbol{v}\|_K = \frac{1}{\Delta t}\sqrt{\boldsymbol{v}^T\boldsymbol{M}_{\text{h}}\boldsymbol{v}} \tag{3.25}$$

may be interpreted as a *kinetic-energy* norm.

In view of the generalized stationarity condition (2.5), it follows that the stable solutions of (3.24) satisfy the minimization problem:

$$\min_{\varphi_{n+1}\in X_h} \{f(\varphi_{n+1}) + I_{C_h}(\varphi_{n+1})\} \tag{3.26}$$

which is equivalent to the constraint minimization problem:

$$\min_{\varphi_{n+1}\in C_h} f(\varphi_{n+1}) \tag{3.27}$$

Adopting the algebraic representation (3.10) of C_h, problem (3.27) may be more explicitly formulated in the form:

$$\min_{\varphi_{n+1}\in X_h} f(\varphi_{n+1}) \tag{3.28}$$

$$\text{subject to } g_\alpha(\varphi_{n+1}) \geqslant 0, \quad \alpha = 1, \ldots, N \tag{3.29}$$

This is a standard nonlinear optimization problem, which may be solved by a variety of methods. One of the most successful methods, which we shall follow, for solving nonlinearly constrained optimization problems is the *sequential quadratic programming* (SQP) method. References for these methods are [51,19,7]. The main idea is to model the nonlinear problem at a given approximate solution x_k by a quadratic programming subproblem, then to use the solution of this subproblem to construct a better approximation x_{k+1}. Thus, by iterating, one obtains a sequence of approximations which converge to a solution x^*. The success of SQP depends on the existence of fast and accurate algorithms for solving quadratic programs [19].

The objective function f is quadratic in the explicit case, Eq. (3.24), and the problem reduces to one of quadratic programming. An essential part of the solution of Eqs. (3.28), (3.29) is the determination of the active constraints. This determination in turn has the effect of resolving the precise sequence of collisions in complex cases involving many fragments such as depicted in Fig. 1.

It should also be noted that, in the explicit case and provided that the mass matrix is diagonal, the global optimization problem decomposes into uncoupled *local* problems, each involving a small number of degrees of freedom Fig. 10. The local problems are set up by first detecting all intersections between segments (faces), an operation which can be carried out efficiently by recourse to quadtree (octree) searches. The intersecting segments (faces) are then grouped in accordance to their respective adjancencies, with every disjoint group defining a local problem. These local problems are then solved independently.

3.7. Geometrical structure

The algorithms just described can be given a revealing geometrical interpretation. In the particular case of explicit integration, (3.20) reduces to

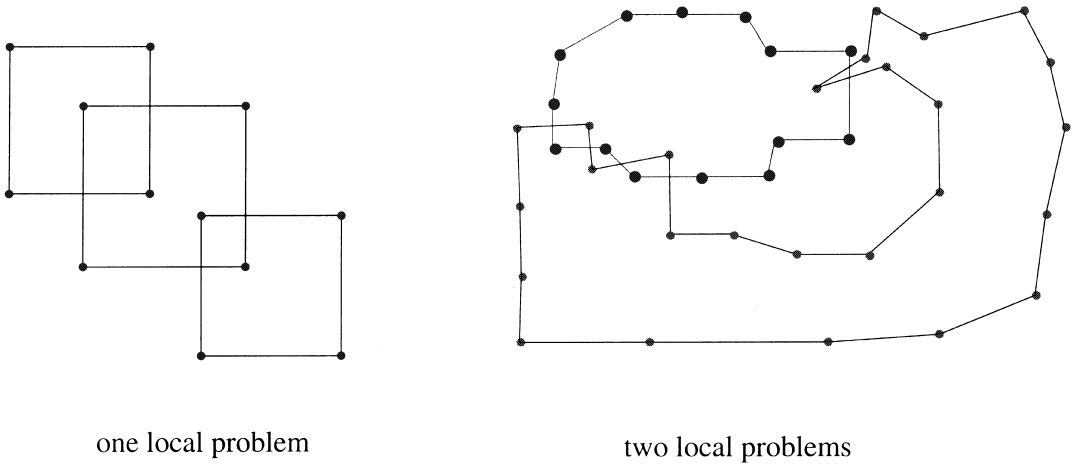

Fig. 10. Decomposition into local problems in the explicit case.

$$\mathbf{0} \in \boldsymbol{M}_h(\boldsymbol{\varphi}_{n+1} - \boldsymbol{\varphi}_{n+1}^{\text{pre}}) + (\Delta t^2/2)\partial I_{C_h}(\boldsymbol{\varphi}_{n+1}), \tag{3.30}$$

which can be further simplified by introducing the normalized variables

$$\boldsymbol{x} = \left[\frac{2}{\Delta t^2}\boldsymbol{M}_h\right]^{1/2} \boldsymbol{\varphi}_{n+1}, \tag{3.31}$$

$$\boldsymbol{y} = \left[\frac{2}{\Delta t^2}\boldsymbol{M}_h\right]^{1/2} \boldsymbol{\varphi}_{n+1}^{\text{pre}}. \tag{3.32}$$

Using this normalization and solving for $\boldsymbol{x}$ in (3.30) gives

$$\boldsymbol{x} = (I + \partial I_{C_h})^{-1}\boldsymbol{y}, \tag{3.33}$$

which, in view of the relation between the resolvent of ∂I_{C_h} and a closest point projection P_{C_h} established in Proposition 2.2, may be recast in the revealing form

$$\boldsymbol{x} \in P_{C_h}\boldsymbol{y}. \tag{3.34}$$

Alternatively, undoing the normalization (3.31) and (3.32) gives the relation

$$\boldsymbol{\varphi}_{n+1} \in P_{C_h}(\boldsymbol{\varphi}_{n+1}^{\text{pre}}), \tag{3.35}$$

where the closest point projection now is to be interpreted in the sense of the kinetic-energy norm (3.34). Evidently, if $\boldsymbol{\varphi}_{n+1}^{\text{pre}} \in C_h$, the closest point projection P_{C_h} returns $\boldsymbol{\varphi}_{n+1} = \boldsymbol{\varphi}_{n+1}^{\text{pre}}$, as required. In view of definition (12), $\boldsymbol{\varphi}_{n+1}$ may also be characterized as the solution of the problem

$$\min_{\boldsymbol{\varphi}_{n+1} \in C_h} \|\boldsymbol{\varphi}_{n+1} - \boldsymbol{\varphi}_{n+1}^{\text{pre}}\|_K^2 \tag{3.36}$$

which is in accordance with (3.27). See Fig. 11.

Remarks.

1. As we shall elaborate in Ref. [23], this algorithm can be written as a product (time splitting) formula. As we mentioned earlier, this procedure has been used in a number of algorithms in plasticity. Additional references are [13,1]. In addition, these algorithms may be viewed in a variational manner, as in Ref. [54].
2. In the course of the algorithm, one may reach, accidentally, points outside the admissible set for which there is no unique projection, but rather the projection is set valued. In these circumstances, the algorithm makes a choice of projection. This is consistent with the sensitive nature of the dynamics with respect to initial conditions.

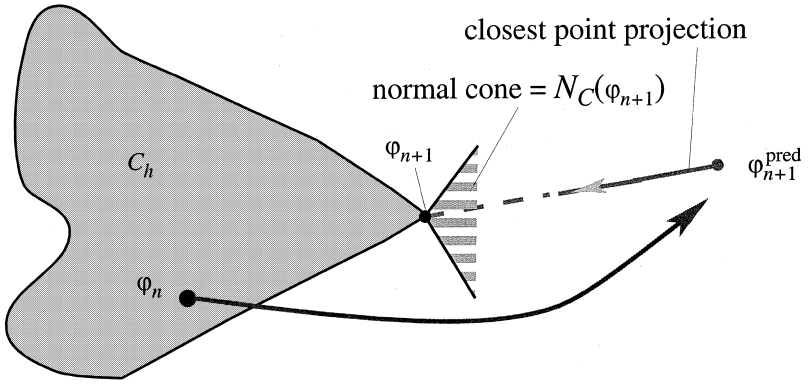

Fig. 11. Predictor–corrector structure of contact algorithm: unconstrained predictor step followed by a projection onto the admissible deformation set.

3. In the course of the algorithm, one may encounter, in exceptional circumstances, a nonsmooth point near which the admissible set is nonconvex. Some examples of this are shown in the figures in the appendix. In such situations, the next step of the algorithm is modified slightly, as is discussed in Ref. [23].

The explicit algorithm is thus found to have a structure similar to that of the closest-point return mapping algorithms of plasticity [37,41]. The predictor $\boldsymbol{\varphi}_{n+1}^{\mathrm{pre}}$, which is computed without regard to contact, will generally wander off the admissible set C_h. This violation of the interpenetration constraint is remedied by returning $\boldsymbol{\varphi}_{n+1}^{\mathrm{pre}}$ to the closest point $\boldsymbol{\varphi}_{n+1}$ on C_h. It bears emphasis, however, that the closest-point projection onto a nonconvex set is set-valued in general and that, consequently, the solution deformation mapping $\boldsymbol{\varphi}_{n+1}$ may be nonunique. This is in sharp contrast to closest-point return mapping algorithms of plasticity, in which the closest-point projection is uniquely determined by virtue of the convexity of the elastic domain.

The lack of uniqueness of the closest-point projection onto C_h may be illustrated by considering a situation in which $\boldsymbol{\varphi}_{n+1}^{\mathrm{pre}}$ lies outside C_h and is equidistant from two possible admissible configurations, as in Fig. 12. Evidently, either of the equidistant admissible configurations lies in the set $P_C(\boldsymbol{\varphi}_{n+1}^{\mathrm{pre}})$ and constitutes a valid solution. One possible selection criterion is to choose one element of the set $P_C(\boldsymbol{\varphi}_{n+1}^{\mathrm{pre}})$ at random, which confers a certain stochastic character to the solution. This stochasticity may not be entirely unphysical, as it is well-known that reentrant corners tend to make the particle-in-a-box system ergodic, as in [50]. In practical calculations, round-off errors are likely to arbitrarily favor one of the possible solutions, thus furnishing an *ad hoc* selection criterion, but one that is consistent with the inherent sharp divergence of nearby trajectories.

The implicit algorithm is also amenable to an analogous geometrical interpretation. To this end, write the stationarity condition (3.22) in the form:

$$-\partial f(\boldsymbol{\varphi}_{n+1}) \in \partial I_{C_h}(\boldsymbol{\varphi}_{n+1}). \tag{3.37}$$

Geometrically, this condition implies that the *energy surface*

$$\varepsilon_h = \{\boldsymbol{\varphi}_h \mid f(\boldsymbol{\varphi}_h) = f(\boldsymbol{\varphi}_{n+1})\} \tag{3.38}$$

is *tangent* to C_h at $\boldsymbol{\varphi}_{n+1}$. This condition is illustrated in Fig. 13. It is also possible, though not essential, to give the above construct a predictor/return-mapping intepretation. Let $\boldsymbol{\varphi}_{n+1}^{\mathrm{unc}}$ be the solution of the unconstrained problem

$$\min_{\boldsymbol{\varphi}_{n+1} \in X_h} f(\boldsymbol{\varphi}_{n+1}) \tag{3.39}$$

whose Euler–Lagrange equations are

$$\mathbf{0} \in \partial f(\boldsymbol{\varphi}_{n+1}). \tag{3.40}$$

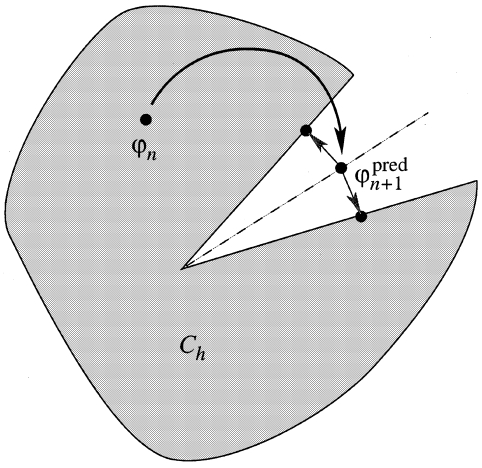

Fig. 12. Schematic of a nonuniqueness situation: the predictor configuration is equidistant from two admissible configurations.

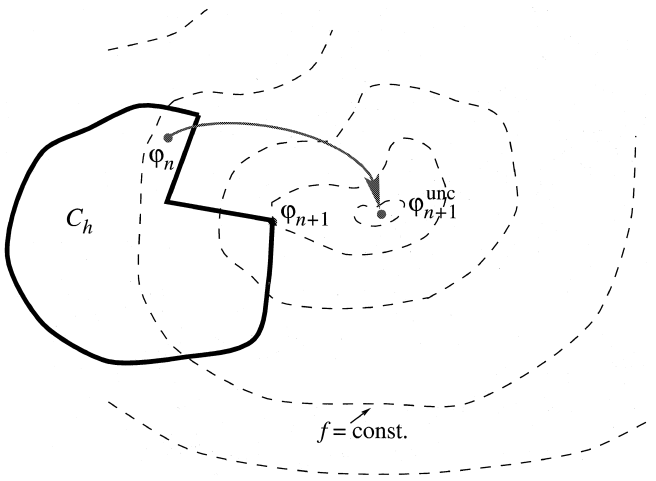

Fig. 13. A possible definition of a return mapping in the implicit case: the unconstrained configuration is returned to the point of tangency between the admissible set and an isoenergy surface.

In the explicit case one simply has $\boldsymbol{\varphi}^{\text{unc}}_{n+1} = \boldsymbol{\varphi}^{\text{pre}}_{n+1}$. Evidently, if $\boldsymbol{\varphi}^{\text{unc}}_{n+1} \in C_h$ it follows that $\mathbf{0} \in \partial I_{C_h}(\boldsymbol{\varphi}^{\text{unc}}_{n+1})$ and (3.36) is trivially satisfied. The return mapping in this case is simply $\boldsymbol{\varphi}_{n+1} = \boldsymbol{\varphi}^{\text{unc}}_{n+1}$. Assume, to the contrary, that $\boldsymbol{\varphi}^{\text{unc}}_{n+1} \notin C_h$. In this case, the return mapping $\boldsymbol{\varphi}^{\text{unc}}_{n+1} \to \boldsymbol{\varphi}_{n+1}$ follows from the tangency construction described above, Fig. 13.

4. Numerical examples

In this section we collect the results of selected numerical tests which demonstrate the robustness and versatility of the algorithms previously described. In all calculations, the bodies are modeled as finitely deforming elastic materials obeying a Neo–Hookean constitutive law extended to the compressible range. The assumed strain energy density has the form

$$W(\boldsymbol{F}) = \frac{\lambda_0}{2}(\log J)^2 - \mu_0 \log J + \frac{\mu_0}{2}\operatorname{tr}(\boldsymbol{C}) \tag{4.1}$$

where $\boldsymbol{F} = \nabla_0 \boldsymbol{\varphi}$ is the deformation gradient; $\boldsymbol{C} = \boldsymbol{F}^T\boldsymbol{F}$ is the right Cauchy–Green deformation tensor; $J = \det(F)$ is the jacobian of the deformation; and λ_0 and μ_0 are material constants. The finite-element implementation of this model accounts for full finite-deformation kinematics, which allows the bodies to deform, translate and rotate freely. The particular choice of material constants used in calculations is: $\lambda_0 = 1.75 \times 10^{11}$, $\mu_0 = 0.801 \times 10^{11}$ and a referential mass density $\rho_0 = 10^3$. All calculations are carried out using the explicit algorithm, $\beta = 0$.

4.1. A four-square body system

Our first example concerns the interaction of four elastic squares, as shown in Fig. 14. The undeformed size of the squares is $L_0 = 1$. The uppermost square is imparted an initial downward velocity $V_0 = 3 \times 10^3$, while the remaining three squares are initially at rest, Fig. 14(a). The squares are disposed such that the first few collisions involve grazing contacts at pairs of corners. This tests the ability of the formulation to effectively arbitrate nonsmooth contact situations. The first such collision occurs at $t \approx 6 \times 10^{-5}$, Fig. 14(b), and involves the two uppermost squares, which meet near a corner. As may be seen in the figure, which shows the velocity field, the incoming square imparts linear and angular momenta on the target square, and itself takes on angular momenta. The angular momenta of the two squares are of opposing signs and cancel

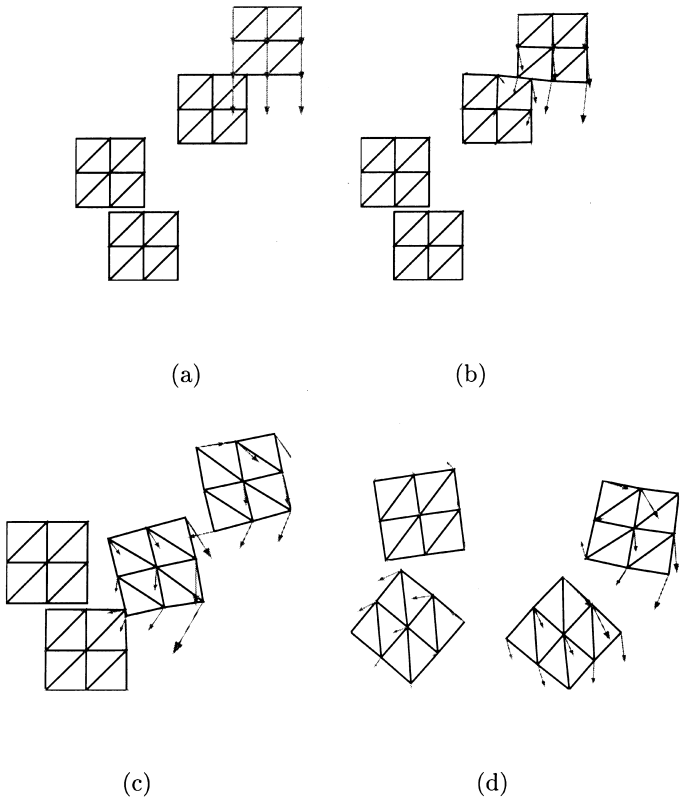

Fig. 14. Dynamics of a four elastic-body system. (a) $t = 0$; (b) $t = 6 \times 10^{-5}$; (c) $t = 62 \times 10^{-5}$; (d) $t = 1.48 \times 10^{-3}$.

each other. It is noteworthy that both linear and angular momenta were exactly preserved throughout the calculation. The subsequent collisions are shown in Fig. 14(b) and (c).

A slow-motion detail of the last collision is shown in Fig. 15. The squares involved in the collision are the two leftmost squares. The upper one is initially at rest. The second square strikes the target square near one of its the corners, Fig. 15(b). Subsequently, that corner slides over the the side of the incoming square until two corners meet. The sliding proceeds beyond this point with the roles of the squares reversed, Fig. 15(c), i.e., with one corner of the incoming square pressing on one side of the target. The ability of the algorithm to resolve sequences of highly nonsmooth contact interactions such as described is particularly noteworthy.

The issue of lack of uniqueness may also be illustrated by arranging the four-square system in the symmetrical initial configuration shown in Fig. 16(a). The figure also shows the initial velocity field, which is designed so that upper-right and lower-left squares come into contact at a corner. Additionally, the upper-right square strikes the remaining two squares. Interestingly, the upper-right and lower-left squares push each other at the corner for a interval of time, Fig. 16(b) and (c). Eventually, symmetry is broken and the upper-right square begins to slide on the right side of the lower-left square, Fig. 16(d).

A detail of the configuration which follows the symmetry breaking is shown in Fig. 17. It bears emphasis that the incoming square could have just as well slid on the upper side of the lower-left square, and the choice of configuration shown in Fig. 17 is arbitrary and probably determined by round-off.

4.2. Scattering of densely packed circular disks and squares

The ability of the algorithm to resolve complex collision sequences is illustrated with the aid of two examples: the scattering of densely packed disks initially at rest in a pool configuration under the action of

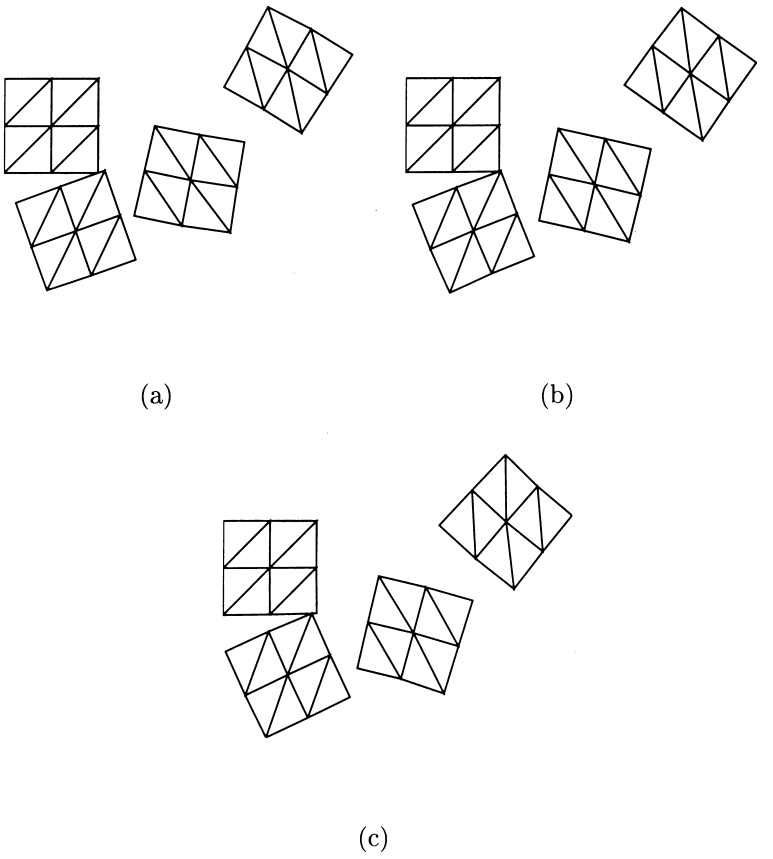

Fig. 15. Four-square problem. Detail of a near corner-corner contact.

an incoming disk; and the scattering of densely packed squares. The early stages of the dynamics of these systems are shown in Figs. 18 and 19.

In the pool configuration, shown in Fig. 18, the undeformed diameter of the disks is $D_0 = 1$. The incoming disk strikes at a speed $V_0 = -1000\mathbf{i}$ in the horizontal direction and is slightly offset downward by a distance of 0.1. The sides of the pool table are themselves flexible and, as may be seen, contain numerous corners, some of which are struck by the disks during their motion. Conditions similar to those encountered in this example are commonly encountered in two-dimensional simulations of granular flows. It should be noted however that, even in extremely dense flows, a simultaneous collision between sixteen particles is indeed and exceedingly rare event. Despite the extreme character of the collision event simulated in the pool example, the contact algorithm successfully resolves the scattering of the disks.

The simulation of the scattering of densely packed squares is even more challenging as it involves a denser arrangements of bodies containing corners. In this calculation, the size of the squares is $L_0 = 1$ and the upper-right square is imparted an initial velocity $V_0 = -3000\mathbf{i} - 3000\mathbf{j}$ in the diagonal direction. Conditions similar to those encountered in this example are encountered in explicit simulations of fracture and fragmentation [10,36]. A particularly challenging aspect of these calculations concerns the resolution of the complex collision sequence undergone by multiple fragments, initially meeting at a point, as they scatter. The ability of the present algorithm to resolve these complex sequences is quite remarkable.

It should be carefully noted that, due to the explicit character of the calculations and the use of a diagonal mass matrix, the contact events just described *decouple* into independent local contact problems each involving but a few degrees of freedom, which considerably speeds-up the calculations.

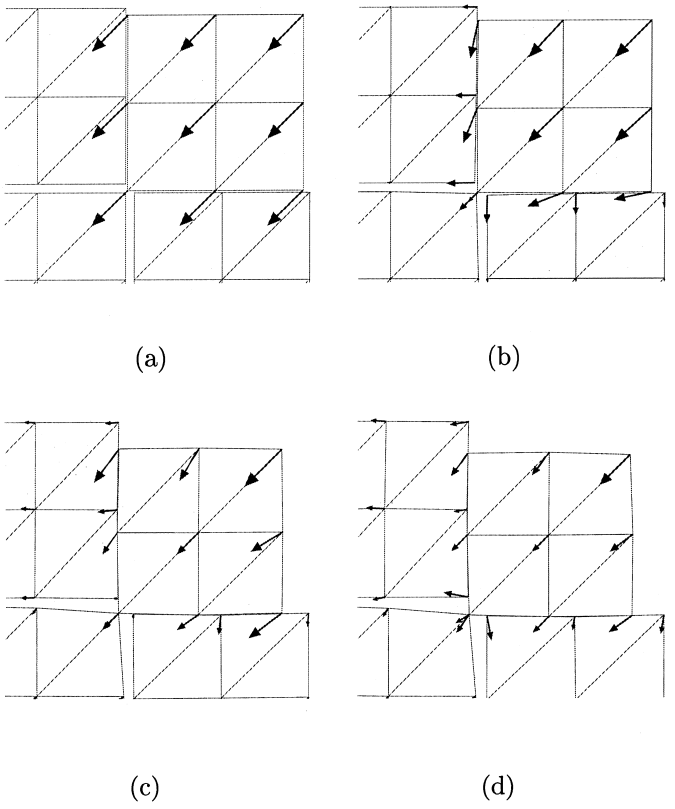

Fig. 16. Four-square problem. Velocity fields.

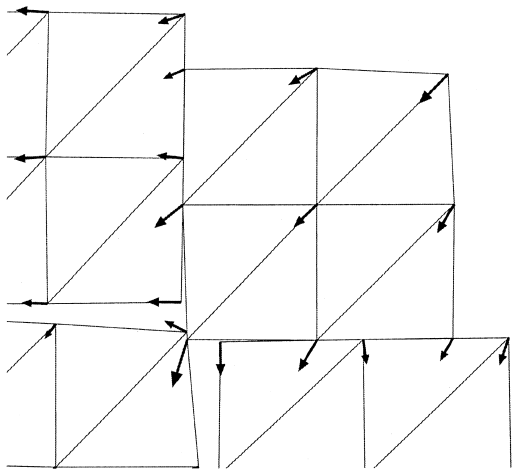

Fig. 17. Four-square problem. Instant at which the symmetry of the corner-corner contact is broken, demonstrating lack of uniqueness of the solution.

4.3. Scattering of packed cubes

The contact interactions that are possible in three dimensions are considerably more complex than in two dimensions. Indeed, two nonsmooth three-dimensional bodies may come in contact in several ways: face on face; edge on edge; vertex on vertex; edge on face; vertex on face; vertex on edge; and so on. When

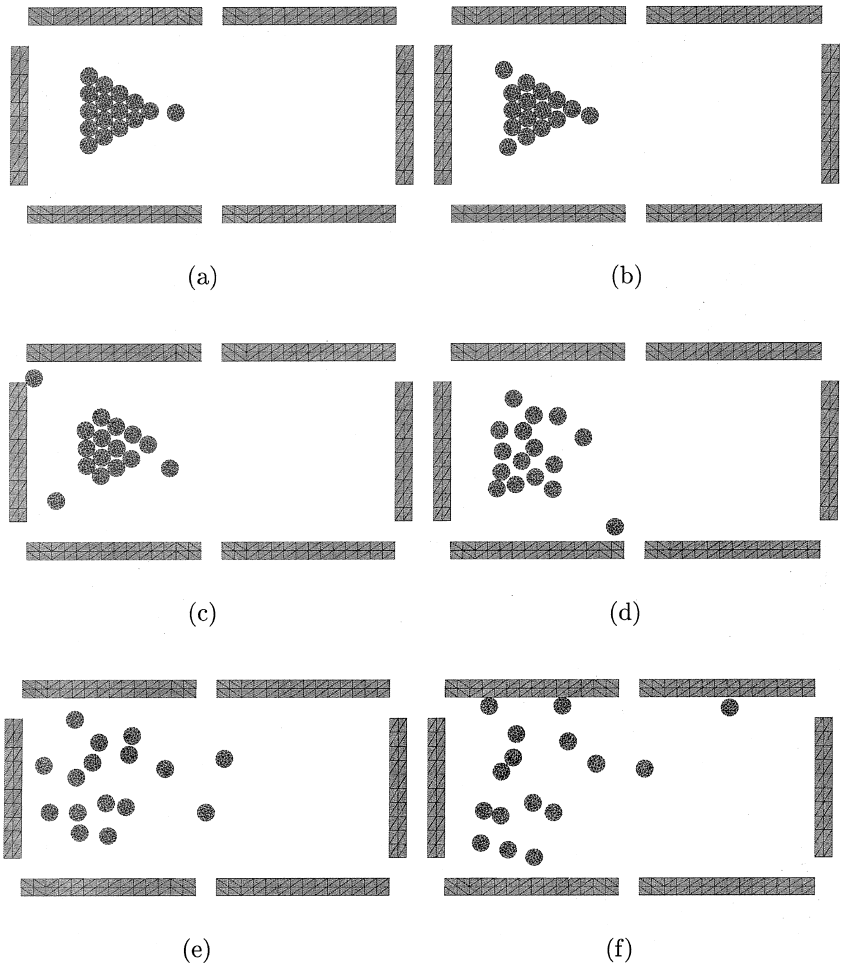

Fig. 18. Pool problem. Trajectories showing multiple collisions and scattering.

more than two bodies come into contact simultaneously, e.g., in the vicinity of a vertex, the number of possible paths which may be followed by the system growths combinatorially. Under these conditions, the staggering complexity of the dynamics defies naive treatment, and the ability to systematically resolve the precise sequence of contact interactions becomes critical. In the present approach, this task is facilitated by the formulation of the contact problem as a nonlinear optimization problem, which reduces the resolution of the collision sequence to the determination of active constraints.

A first test which illustrates the ability of the present approach to deal with nonsmooth situations in three dimensions concerns the collision of two cubes which come together symmetrically at one edge, Fig. 20. In this calculation, the cubes have a size $L_0 = 5$, their elastic moduli are $E = 0.778 \times 10^5$, $\nu = 0.25$, and the mass density is $\rho = 3690$. The time step used in the calculations is $\Delta t = 10^{-4}$. The right incoming cube is given an initial velocity $v_1 = -0.3, v_2 = -0.3, v_3 = 0$. As may be seen from Fig. 20, which shows several snapshots of the collision, the cubes deform elastically under the impact and interact closely for some time before eventually separating. The example shown in Fig. 21 concerns a similar case in which a pair of cubes come in contact at two vertices. The upper right incoming cube in the figure has a initial velocity of $v_1 = -0.3, v_2 = -0.3, v_3 = -0.3$, and the target cube is supported so as to restrain its motion. In this example, the incoming cube slides over the target vertex. The target cube undergoes large deformations during the impact. The incoming cube is imparted an angular velocity and eventually separates from the target cube along a much deflected trajectory, Fig. 21. It bears emphasis that the contact configurations in these two examples are nonsmooth and that normals are undefined in both cases.

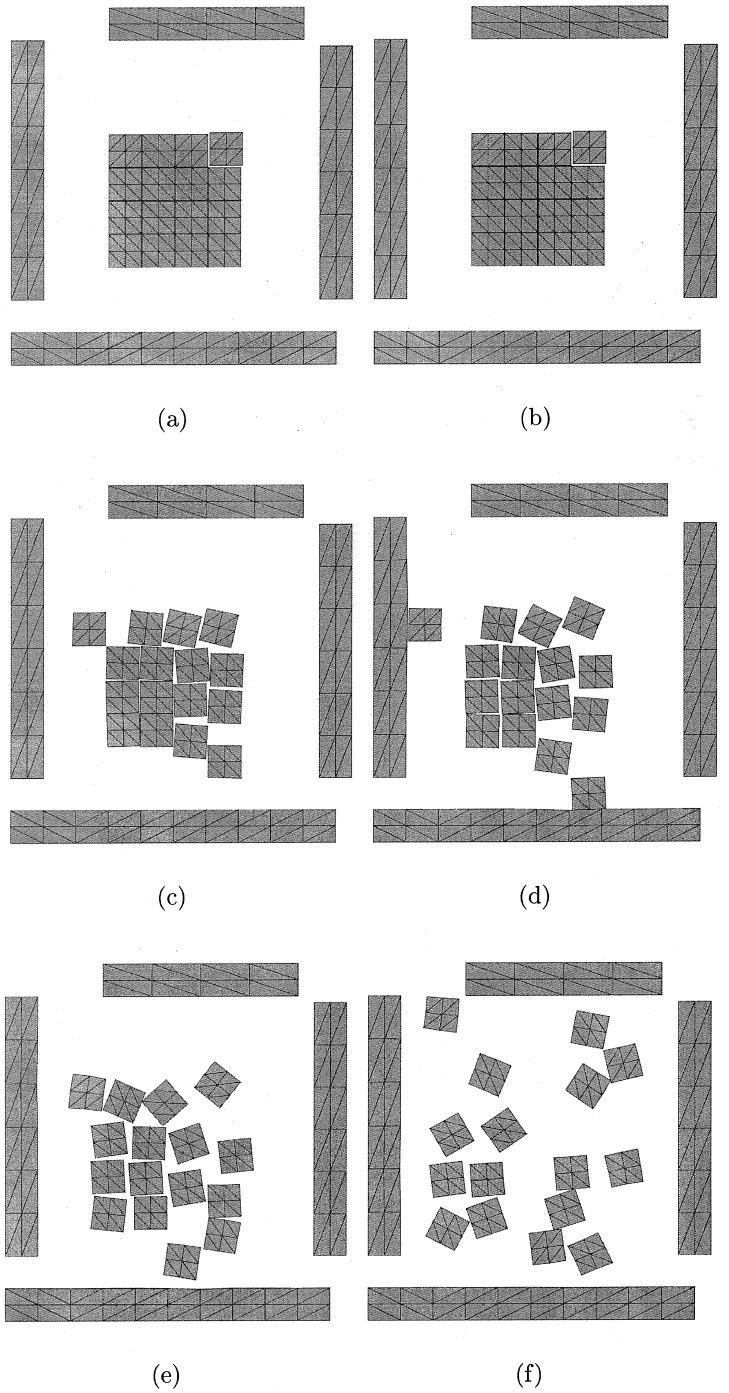

Fig. 19. Scattering of initially packed square bodies. Trajectories showing multiple collisions and scattering.

A test problem which illustrates the ability of the nonsmooth contact algorithm to resolve complex collision sequences between multiple bodies in three dimensions concerns the scattering of eight packed cubes, Fig. 22(a). The cubes are of unit size and are initially disposed at a relative distance of 7×10^{-3}. The elastic constants employed in the analysis are: $E = 0.778 \times 10^{11}$, $v = 0.25$, and the mass density is $\rho = 3690$. The time step used in the calculations is $\triangle t = 10^{-7}$. The cube arrangement is disturbed by imparting an initial velocity $v_1 = 30$, $v_2 = 20$, $v_3 = -50$, to one of the cubes. The incoming cube comes in contact with the

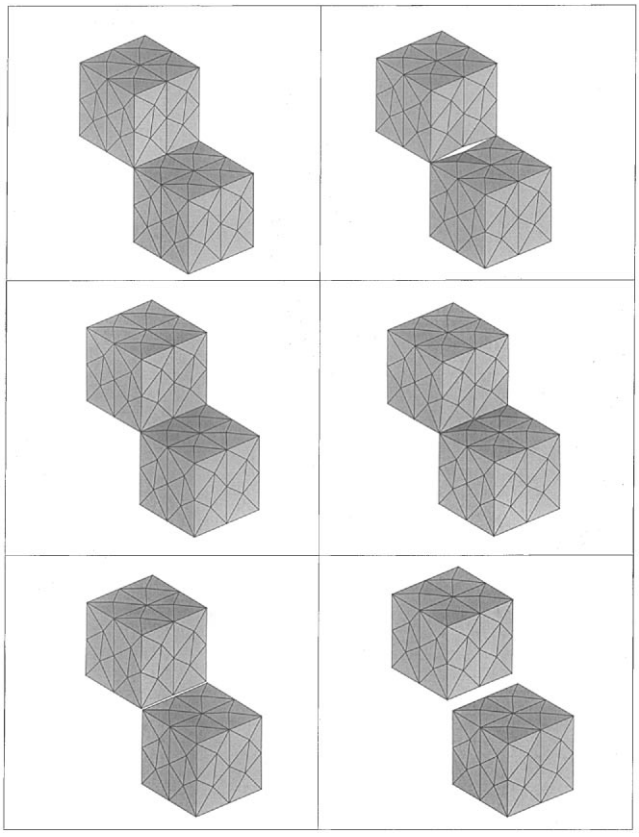

Fig. 20. Two cubes colliding at two edges.

other cubes and the ensemble undergoes a complex sequence of collisions before eventually scattering, Fig. 22(a).

It should be noted that initially eight different nonmooth bodies are disposed at close range of each other in the vicinity of the common vertex. Evidently, methods based on the use of normals and gap functions are not applicable to such a case. By contrast, the ability of the present method to resolve the complex trajectory of the cubes is remarkable.

5. Summary and conclusions

We have applied nonsmooth analysis (see Ref. [14]) to the development of robust contact algorithms capable of dealing with complex contact situations involving several bodies with corners. We have specifically addressed contact geometries for which *neither normals nor gap functions may be defined*, which precludes the application of most contact algorithms proposed to date. Such situations arise in applications such as: fragmentation, where angular fragments undergo complex collision sequences before they scatter; granular flows, and others.

The resulting algorithms bear a noteworthy resemblance to those which are suggested by the mathematical theory of plasticity (see, e.g., Refs. [35,37,41]), specially as regards the use of *closest-point projections*. However, it should be noted that the admissible sets which arise in contact problems are generally *nonconvex*, which precludes the direct application of convex analysis.

The theory accords all bodies an equal role without differentiating between master and slave bodies. This is particularly advantageous in situations such that several angular bodies meet near a point, as for these configurations it is not generally possible to classify the bodies as master or slave.

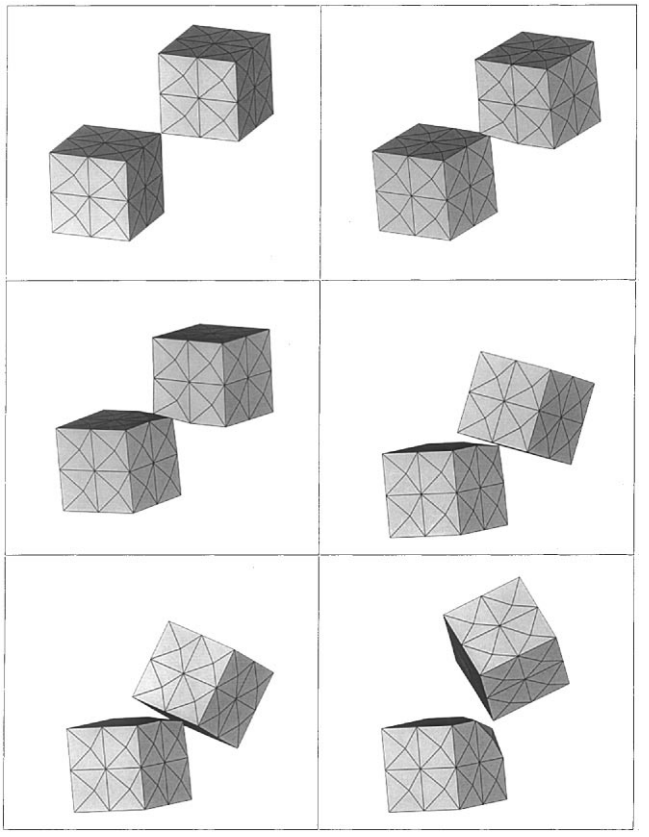

Fig. 21. Two cubes colliding at two vertices.

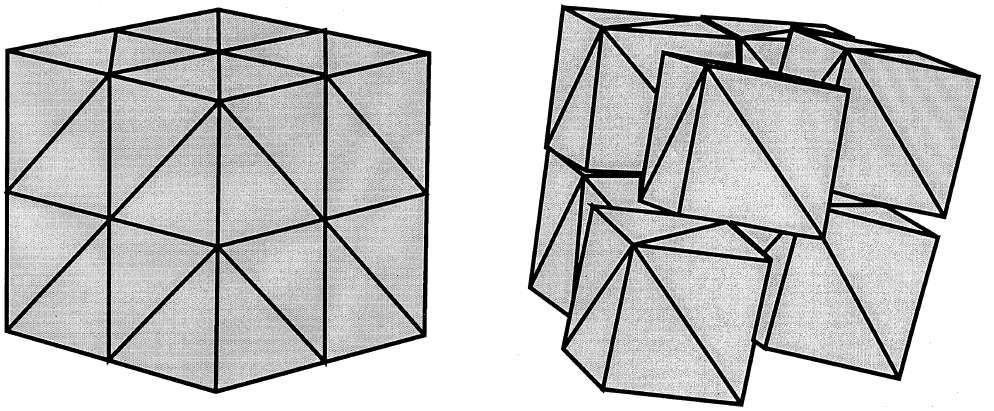

Fig. 22. Three-dimensional simulation of colliding cubes. Tetrahedral elements are used in the calculations. The mesh lines shown in the figure are for visualisation purposes only.

In order to reap the full benefit of nonsmooth analysis, including the robustness of closest-point projections, it is necessary to treat the contact interactions in a fully implicit manner. The remaining force terms may be treated either implicitly or explicitly, leading to implicit/implicit and explicit/implicit algorithms. In the case of the explicit/implicit algorithm, the use of a diagonal mass matrix results in the decoupling of the global contact problem into independent *local* contact problems each typically involving a few degrees of freedom. These local problems can efficiently be set up using quadtree/octree searches. The

local character of the contact algorithm in the context of explicit dynamics considerably speeds-up the calculations.

We have demonstrated the robustness and versatility of the nonsmooth contact algorithms developed in this paper with the aid of selected two and three-dimensional applications, including the scattering of densely packed disks, squares and cubes.

Acknowledgements

CK, JEM and MO are grateful to the AFOSR for partial support through Caltech's MURI on Mathematical Infrastructure for Robust Virtual Engineering. CK and MO are grateful to the DoE for partial support through Caltech's ASCI Center for the Simulation of the Dynamic Response of Materials. MO also wishes to gratefully acknowledge the support of the Army Research Office through grant DAAH04-96-1-0056.

Appendix A. Formulation of the contact constraints

In this appendix we collect implementation details pertaining to the evaluation of the contact constraints. The boundaries of the solids are assumed to be triangulated and oriented so as to define their interior and exterior domains unambiguously. Each pair of simplices in the boundary triangulation defines a – possibly inactive – constant constraint. Given a pair of boundary simplices, we wish to define a simple function g of the boundary node positions such that $g \geqslant 0$ when the simplices do not interpenetrate and $g < 0$ otherwise. To this end, we differentiate explicitly between the two and three-dimensional cases.

A.1. The two-dimensional case

The geometry of an intersecting pair of boundary segments is shown in Fig. 23. By convention, all boundaries are oriented counterclockwise so that the interior of a body is on the left of its boundary. The ends of the segments and their point of intersection $\boldsymbol{x}_0$ define two triangles: one, $\{\boldsymbol{x}_1, \boldsymbol{x}_0, \boldsymbol{x}_4\}$, is oriented counterclockwise and encloses a positive area A of interpenetration; the remaining triangle, $\{\boldsymbol{x}_3, \boldsymbol{x}_0, \boldsymbol{x}_2\}$, is oriented clockwise and encloses an admissible negative area.

A first choice of constraint function is, therefore,

$$A = \frac{(\boldsymbol{x}_{31} \times \boldsymbol{x}_{34}) \cdot (\boldsymbol{x}_{21} \times \boldsymbol{x}_{24})}{(\boldsymbol{x}_{34} \times \boldsymbol{x}_{21}) \cdot \boldsymbol{k}}, \tag{A.1}$$

where we write $\boldsymbol{x}_{ij} = \boldsymbol{x}_j - \boldsymbol{x}_i$, and $\boldsymbol{k}$ is the unit vector normal to the plane. It is evident from Eq. (A.1) that A is a rational function of $\{\boldsymbol{x}_1, \boldsymbol{x}_2, \boldsymbol{x}_3, \boldsymbol{x}_4\}$. However, it is possible to reduce the constraint function to a

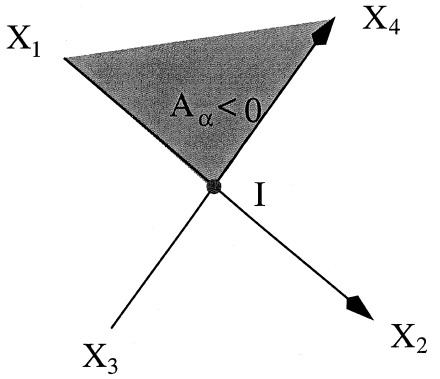

Fig. 23. Analytical formulation of nonsmooth contact constraints.

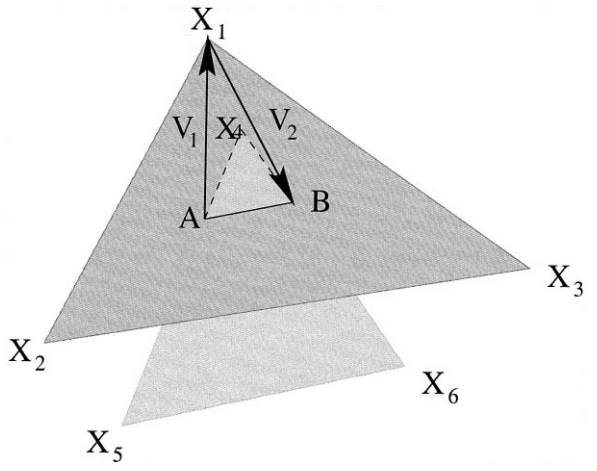

Fig. 24. Analytical formulation of nonsmooth contact constraints.

polynomial form by noting that the denominator of (A.1) is necessarily positive. It therefore follows that the numerator of Eq. (A.1) may alternatively be taken as constraint function, with the result:

$$g = (\boldsymbol{x}_{31} \times \boldsymbol{x}_{34}) \cdot (\boldsymbol{x}_{21} \times \boldsymbol{x}_{24}) \tag{A.2}$$

which is polynomial, as advertised. This algebraic simplification reduces the two-dimensional contact problem to a nonlinear optimization problem with polynomial constraints.

A.2. The three-dimensional case

The three-dimensional case amenable to a similar treatment. The geometry of an intersecting pair of boundary facets is shown in Fig. 24. By convention, all boundary facets are oriented counterclockwise when seen from the outside of the body, so that the interior of a body is below its boundary.

We consider a pair of triangles in space defined by vertices $\{\boldsymbol{x}_1, \boldsymbol{x}_2, \boldsymbol{x}_3\}$ and $\{\boldsymbol{x}_4, \boldsymbol{x}_5, \boldsymbol{x}_6\}$, respectively. Let $\boldsymbol{A}$ and $\boldsymbol{B}$ denote the two points of intersection between the triangles, which follow as;

$$\boldsymbol{A} = \boldsymbol{x}_5 - \frac{\boldsymbol{x}_{15} \cdot (\boldsymbol{x}_{12} \times \boldsymbol{x}_{23})}{\boldsymbol{x}_{45} \cdot (\boldsymbol{x}_{12} \times \boldsymbol{x}_{23})} \boldsymbol{x}_{45}, \tag{A.3}$$

$$\boldsymbol{B} = \boldsymbol{x}_6 - \frac{\boldsymbol{x}_{16} \cdot (\boldsymbol{x}_{12} \times \boldsymbol{x}_{23})}{\boldsymbol{x}_{46} \cdot (\boldsymbol{x}_{12} \times \boldsymbol{x}_{23})} \boldsymbol{x}_{46}. \tag{A.4}$$

Let $\boldsymbol{v}_1 = \boldsymbol{x}_1 - \boldsymbol{A}$ and $\boldsymbol{v}_2 = \boldsymbol{B} - \boldsymbol{x}_1$, Fig. 24. Define the volume:

$$V = (\boldsymbol{v}_2 \times \boldsymbol{v}_1) \cdot \boldsymbol{x}_{41}. \tag{A.5}$$

As in the two-dimensional case, the condition $V > 0$ precludes interpenetration and, therefore, V may be taken as the constraint function g. In view of Eqs. (A.3) and (A.4), it is evident that V is a rational function of $\{\boldsymbol{x}_1, \boldsymbol{x}_2, \boldsymbol{x}_3, \boldsymbol{x}_4, \boldsymbol{x}_5, \boldsymbol{x}_6\}$. However, the denominator of V is always positive, and the numerator of V, which is polynomial, can alternatively be taken as constraint function. This reduces the three-dimensional contact problem to a nonlinear optimization problem with polynomial constraints.

References

[1] F. Armero, J.C. Simo, A-priori stability estimates and nconditionally stable product formula algorithms for non-linear coupled thermoplasticity, International Journal of Plasticity 9 (1993) 149–182.

[2] K.J. Bathe, Some remarks and references on recent developments in finite-element analysis procedures, Computers and Structures 40 (2) (1991) 201–202.

[3] K.J. Bathe, P.A. Bouzinov, On the constraint function-method for contact problems. Computers and Structures 64 (5–6) (1997) 1069–1085.
[4] K.J. Bathe, A. Chaudhary, A solution method for planar and axisymmetric contact problems, International Journal for Numerical Methods in Engineering 21 (1) (1985) 65–88.
[5] K.J. Bathe, S. Mijailovich, Finite-element analysis of frictional contact problems, Journal de Mecanique Theorique et Appliquée 7 (S1) (1988) 31–45.
[6] T. Belytschko. An overview of semidiscretization and time integration procedures, in: T. Belytschko, T.J.R. Hughes (Eds.), Computational Methods for Transient Analysis, ch. 1, North-Holland, Amsterdam, 1983, pp. 1–65.
[7] P.T. Boggs, J.W. Tolle, Sequential quadratic programming, Acta Numerica 1 (1995) 1–51.
[8] H. Brezis. Opérateurs maximaux monotones et semi-groupes de contractions dans les espaces de Hilbert, North-Holland, Amsterdam, 1973.
[9] H. Brezis, A. Pazy, Semigroups of nonlinear contractions on convex sets, Journal of Functional Analysis 6 (1970) 237–281.
[10] G.T. Camacho, M. Ortiz, Computational modelling of impact damage in brittle materials, International Journal of Solids and Structures 33 (20–22) (1996) 2899–2938.
[11] N.J. Carpenter, R.L. Taylor, M.G. Katona, Lagrange constraints for transient finite-element surface-contact, International Journal for Numerical Methods in Engineering 32 (1) (1991) 103–128.
[12] A.B. Chaudhary, K.J. Bathe, A solution method for static and dynamic analysis of contact problems with friction. Computers and Structures 3-dimensional 6 (1986) 855–873.
[13] A.J. Chorin, T.J.R. Hughes, J.E. Marsden, M. McCracken, Product formulas and numerical algorithms, Comm. Pure Appl. Math 31 (1978) 205–256.
[14] F.H. Clarke, Optimization and nonsmooth analysis, Wiley, New York, 1983.
[15] G. Crandall, A. Pazy, Semi-groups of nonlinear contractions and dissipative sets, Journal of Functional Analysis 6 (1969) 376–418.
[16] G. Crandall, A. Pazy, On accretive sets in Banach spaces, Journal of Functional Analysis 5 (1970) 204–217.
[17] T. Endo, J.T. Oden, E.B. Becker, T. Miller, A numerical-analysis of contact and limit-point behavior in a class of problems of finite elastic-deformation, Computers and Structures 18 (5) (1984) 899–910.
[18] A.L. Eterovic, K.J. Bathe, On the treatment of inequality constraints arising from contact conditions in finite-element analysis 2 (1991) 203–209.
[19] D. Goldfarb, A. Idnani, A numerically stable dual method for solving strictly quadratic programs, Mathematical Programming 27 (1983) 1–33.
[20] C.M. Hoffmann. Geometric and solid modeling, Morgan Kaufmann Publishers, California, San Mateo, 1989.
[21] T.J.R. Hughes. Analysis of transient algorithms with particular reference to stability behavior, Computational Methods for Transient Analysis, North-Holland, Amsterdam, 1983, pp. 67–155.
[22] J.W. Ju, R.L. Taylor, A perturbed lagrangian formulation for the finite-element solution of nonlinear frictional contact problems, Journal de Mecanique Theorique et Appliquee 7 (S1) (1988) 1–14.
[23] C. Kane, J.E. Marsden, M. Ortiz, On the analysis of nonsmooth contact, in preparation.
[24] Y. Komura, Nonlinear semigroups in Hilbert space, Journal of the Mathematical Society of Japan 19 (1967) 493–507.
[25] Y. Komura, Differentiability of nonlinear semigroups, J. Math. Soc. Japan 21 (1969) 375–402.
[26] C.Y. Lee, J.T. Oden, A priori error estimation of hp-finite element approximations of frictional contact problems with normal compliance, International Journal of Engineering Science 31 (6) (1993) 927–952.
[27] C.Y. Lee, J.T. Oden, Theory and approximation of quasi-static frictional contact problems, Computer Methods in Applied Mechanics and Engineering 106 (3) (1993) 407–429.
[28] C.Y. Lee, J.T. Oden, A-posteriori error estimation of hp finite-element approximations of frictional contact problems, Computer Methods in Applied Mechanics and Engineering 113 (1–2) (1994) 11–45.
[29] J.E. Marsden, T.S. Ratiu, Mechanics and Symmetry, Texts in applied mathematics, vol. 17, Springer, Berlin, 1994.
[30] J.A.C. Martins, J.T. Oden, Existence and uniqueness results for dynamic contact problems with nonlinear normal and friction interface laws, Nonlinear Analysis Theory Methods and Applications 11 (3) (1987) 407–428.
[31] E.A.D. Neto, K. Hashimoto, D. Peric, D.R.J. Owen, A phenomenological model for frictional contact accounting for wear effects, Philosophical Transactions of the Royal Society of London A 354 (1996) 373–389.
[32] B. Nouromid, A 2-level iteration method for solution of contact problems, 54 2-level (2) (1986) 131–144.
[33] J.T. Oden, T.L. Lin, On the general rolling-contact problem for finite deformations of a viscoelastic cylinder, Computer Methods in Applied Mechanics and Engineering 57 (3) (1986) 297–367.
[34] J.T. Oden, E.B. Pires, Algorithms and numerical results for finite-element approximation of contact problems with non-classical friction laws, Computers and Structures 19 (1/2) (1984) 137–147.
[35] M. Ortiz, Topics in constitutive theory for inelastic solids, Ph.D. thesis, University of California at Berkeley, Berkeley, 1981.
[36] M. Oritz, Computational micromechanics, Computational Mechanics 18 (1996) 321–338.
[37] M. Oritz, P.M. Pinsky, R.L. Taylor, Operator split methods for the numerical solution of the elastoplastic dynamic problem, Computer Methods in Applied Mechanics and Engineering 39 (2) (1983) 137–157.
[38] P. Papadopoulos, R.L. Taylor, A mixed formulation for the finite-element solution of contact problems, Computer Methods in Applied Mechanics and Engineering 39 (2) (1983) 137–157.
[39] P. Papadopoulos, R.L. Taylor, A simple algorithm for finite-element analysis of contact problems, Computers and Structures A simple algorithm for 3-dimensional 6 (1993) 1107–1118.
[40] D. Peric, D.R.J. Owen, Computational model for contact problems with friction based on the penalty method, International Journal for Numerical Methods in Engineering 3-D 6 (1992) 1289–1309.

[41] P.M. Pinsky, M.Ortiz, R.L. Taylor, Operator split methods for the numerical solution of the finite-deformation elastoplastic dynamic problem, Computers and Structures 17 (3) (1983) 345–359.
[42] E.B. Pires, J.T. Oden, Analysis of contact problems with friction under oscillating loads, Computer Methods in Applied Mechanics and Engineering 3 (1983) 337–362.
[43] P. Rabier, J.A.C. Martins, J.T. Oden, L. Campos, Existence and local uniqueness of solutions to contact problems in elasticity with nonlinear friction laws, International Journal of Engineering Science 24 (11) (1986) 1755–1768.
[44] P.J. Rabier, J.T. Oden, Solution to Signorini-like contact problems through interface models 1. Preliminaries and formulation of a variational equality, Nonlinear Analysis Theory Methods and Applications 11 (12) (1987) 1325–1350.
[45] P.J. Rabier, J.T. Oden, Solution to Signorini-like contact problems through interface models. Part 2. Existence and uniqueness theorems, Nonlinear Analysis Theory Methods and Applications 12 (1) (1988) 1–17.
[46] R. Radovitzky, M. Ortiz, Error estimation and adaptive meshing in strongly nonlinear dynamic problems, Comput. Methods Appl. Mech. Engrg. 172 (1999) 203–240.
[47] R.T. Rockafellar, Convex analysis, Princeton, NJ, 1970.
[48] J.C. Simo, P. Wriggers, K.H. Schweizerhof, R.L. Taylor, Finite deformation post-buckling analysis involving inelasticity and contact constraints, International Journal for Numerical Methods in Engineering 23 (5) (1986) 779–800.
[49] J.C. Simo, P. Wriggers, R.L. Taylor, A perturbed lagrangian formulation for the finite-element solution of contact problems, Computer Methods in Applied Mechanics and Engineering 50 (2) (1985) 163–180.
[50] Y.G. Sinai, Topics in ergodic theory, Princeton Mathematical Series, vol. 44, Princeton University Press, Princeton, NJ, 1994.
[51] P. Spellucci, A new technique for inconsistent QP problems in the SQP method, Technical University at Darmstadt, 1993.
[52] E. Stein, P. Wriggers, Calculation of impact contact problems of thin elastic shells taking into account geometrical nonlinearities within the contact region, Computer Methods in Applied Mechanics and Engineering 34 (1–3) (1982) 861–880.
[53] R.L. Taylor, P. Papadopoulos, On a finite-element method for dynamic contact impact problems, International Journal for Numerical Methods in Engineering 36 (12) (1993) 2123–2140.
[54] J.M. Wendlandt, J.E. Marsden, Mechanical integrators derived from a discrete variational principle, Physica 106 (1997) 223–246.
[55] L. White, J.T. Oden, Dynamics and control of viscoelastic solids with contact and friction effects, Nonlinear Analysis Theory Methods and Applications 13 (4) (1989) 459–474.
[56] P. Wriggers, M. Imhof, On the treatment of nonlinear unilateral contact problems Archive of Applied Mechanics Ingenieur Archiv2 (1993) 116–129.
[57] P. Wriggers, C. Miehe, Contact constraints within coupled thermomechanical analysis – a finite-element model, Computer Methods in Applied Mechanics and Engineering 113 (3–4) (1994) 301–319.
[58] P. Wriggers, O. Scherf, An adaptive finite-element algorithm for contact problems in Plasticity, Computational Mechanics 17 (1–2) (1995) 88–97.
[59] P. Wriggers, J.C. Simo, A note on tangent stiffness for fully nonlinear contact problems, Communications in Applied Numerical Methods 1 (5) (1985) 199–203.
[60] P. Wriggers, T.V. Van, E. Stein, Finite-element formulation of large deformation impact-contact problems with friction, Computers and Structures 37 (3) (1990) 319–331.
[61] P. Wriggers, G. Zavarise, Application of augmented lagrangian techniques for nonlinear constitutive laws in contact interfaces, Communications in Numerical Methods in Engineering 9 (10) (1993) 815–824.
[62] P. Wriggers, G. Zavarise, Thermomechanical contact – a rigorous but simple numerical approach, Computers and Structures1 (1993) 47–53.
[63] P. Wriggers, G. Zavarise, On contact between beams undergoing large deflections, Communications in Numerical Methods in Engineering 3-dimensional (6) (1997) 429–438.
[64] G. Zavarise, P. Wriggers, B.A. Schrefler, On augmented lagrangian algorithms for thermomechanical contact problems with friction, International Journal for Numerical Methods in Engineering 38 (17) (1995) 2929–2949.
[65] G. Zavarise, P. Wriggers, E. Stein, B.A. Schrefler, A numerical-model for thermomechanical contact based on microscopic interface laws, Mechanics Research Communications 19 (3) (1992) 173–182.
[66] G. Zavarise, P. Wriggers, E. Stein, B.A. Schrefler, Real contact mechanisms and finite-element formulation – a coupled thermomechanical approach, International Journal for Numerical Methods in Engineering 35 (4) (1992) 767–785.
[67] F. Schuricht, A variational approach to obstacle problems for shearable nonlinearly elastic rods, Archive for Rational Mechanics and Analysis 140 (2) (1997) 103–159.
[68] F. Schuricht. Regularity of shearable nonlinearly elastic rods in obstacle problems. Technical Report 1997/29, Max Planck Institut für Mathematik in den Naturwissenschaften, Leipzig, Germany, 1997.
[69] T.A. Laursen, S. Govindjee, A note on the treatment of frictionless contact between nonsmooth surfaces in fully nonlinear problems, Communications in Numerical Methods in Engineering 10 (11) (1994) 869–878.